Y 3.N21/5:6/3351

GOVT. DOC.

BUSINESS AND TECHNICAL DEPT.
Apr 13

NACA TN 3351

NATIONAL ADVISORY COMMITTEE FOR AERONAUTICS

TECHNICAL NOTE 3351

PLASTIC DEFORMATION OF ALUMINUM SINGLE CRYSTALS AT ELEVATED TEMPERATURES

By R. D. Johnson, A. P. Young, and A. D. Schwope

Battelle Memorial Institute

NACA

Washington

April 1955

NATIONAL ADVISORY COMMITTEE FOR AERONAUTICS

TECHNICAL NOTE 3351

PLASTIC DEFORMATION OF ALUMINUM SINGLE CRYSTALS AT ELEVATED TEMPERATURES

By R. D. Johnson, A. P. Young, and A. D. Schwope

SUMMARY

This report describes the results of a comprehensive study of plastic deformation of aluminum single crystals over a wide range of temperatures. The results of constant-stress creep tests have been reported for the temperature range from 400° to 900° F. For these tests, a new capacitance-type extensometer was designed. This unit has a range of 0.30 inch over which the sensitivity is very nearly linear and can be varied from as low a sensitivity as is desired to a maximum of 10 microinches per millivolt with good stability.

In constant-load creep tests at temperatures up to 1,100° F, four additional slip planes (the (100), (311), (110), and (211)) have been observed, besides the customary (111) plane. The (311) slip plane has been observed above 300° F; the (100), above 500° F; the (211), above 700° F; and the (110), only at 1,000° F.

The stress-strain curve has been determined in constant-load-rate tests at temperatures of 82°, 500°, and 1,100° F for single crystals of two purities, 99.99+ percent and 99.95 percent aluminum.

Experiments were carried out to investigate the effect of small amounts of prestraining, by two different methods, on the creep and tensile properties of these aluminum single crystals. Two high-resolution X-ray techniques used to detect and to follow the strain in these experiments showed a definite polygonization of the crystalline lattice during creep.

Light microscopy has been employed to observe the details of the process of kinking. Electron microscopy has been used with various replica techniques to investigate the complex nature of the slip bands resulting from plastic deformation at elevated temperatures. From these observations, it has been concluded that plastic deformation takes place predominantly by slip which is accompanied by the mechanisms of kinking and polygonization.

INTRODUCTION

This investigation has been directed toward the problem of determining the mechanisms of creep. This required that a number of different approaches be employed in attacking the problem. Reliable creep data had to be obtained over a wide range of temperatures. Then perturbations or small changes had to be introduced into the specimens to study their effects on the deformation characteristics. Examples of such perturbations are a small change in purity or a small amount of prestraining. In addition, it was necessary to observe the changes in the specimens resulting from plastic deformation. This can be done on the surface by light microscopy, or, on an even finer scale, by electron microscopy. The deformation can be studied below the surface by high-resolution X-ray diffraction methods.

Previous portions of this investigation have included a survey of creep in metals (ref. 1), a study of the plastic and elastic properties of high-purity aluminum single crystals at room temperature (ref. 2), and a determination of the creep and tensile properties of these aluminum single crystals from room temperature to 400° F (ref. 3). This portion of the investigation has been concerned primarily with the plastic properties, both creep and tensile, over a wide range of temperatures up to and including 1,100° F.

Normal X-ray back-reflection Laue photographs were used for orientation determination. This same method can be used to identify the operative slip system when tests are conducted in the temperature range wherein more than one type of slip plane may operate. This was found to be necessary in aluminum, where the slip plane might be (111), (100), or (211) at elevated temperatures.

The use of electron microscopy in studying the deformation of metals on a submicroscopic scale is just coming into prominent and accepted use. Although research of this type has been carried on for the past few years, better and more reliable methods of replication have greatly enhanced the use of the electron microscope in this particular application. Most of these studies to date have been on polycrystalline materials deformed in tensile tests or by bending. This effort represents one of the first to study the plastic deformation of single-crystal specimens by creep with electron microscopy and replica techniques.

This investigation was conducted at Battelle Memorial Institute under the sponsorship and with the financial assistance of the National Advisory Committee for Aeronautics. The authors wish to thank Messrs. G. D. McDowell, W. B. Wilson, and J. R. Doig for performing the X-ray work throughout the course of the investigation. Thanks are also

extended to Mr. C. L. Seale for his part in developing the capacitance strain gage and associated electronic equipment and to Mr. R. D. Smith for carrying out the testing program.

SYMBOLS

$d = 1 + \epsilon$

L	prefix to crystal number, indicating 99.95 percent purity
P,S	prefix to crystal number, indicating 99.99^+ percent purity
α,β,χ	angles between three cube planes and specimen axis
γ	resolved shear strain
ϵ	tensile strain
λ	angle between slip direction and specimen axis
σ	tensile stress
τ	resolved shear stress
ϕ	angle between normal to slip plane and specimen axis

EQUIPMENT

Testing Facilities

The general equipment for performing creep tests and constant-load tests at elevated temperatures has been described in detail elsewhere (ref. 3). Three creep units were designed to employ direct axial loading through a fixed ball-seat arrangement. Two units were modified to allow loading through a lever arm with a 9:1 arm ratio. These units were used for constant-load-rate tests in which the load was applied by vibrating lead shot along a trough into a weight pan at the end of the lever arm at approximately a constant rate. This equipment was housed in a constant-temperature room in which the temperature was maintained at $82^\circ \pm 2^\circ$ F. Each creep unit was equipped with an electric-resistance-type furnace, either in one piece or of the split type. The power to each furnace was controlled by a Variac connected to a Honeywell controller.

Constant-Stress Device

One of the creep units previously used for direct loading has been converted to a special lever-arm arrangement. The mechanics of this type of arrangement have been described by Cottrell and Aytekin (ref. 4). In the deformation of single crystals, the slip direction rotates toward the tension axis as extension takes place. In order to maintain a constant resolved shear stress, that is, the component of the tensile stress resolved in the slip plane in the slip direction, it is necessary to reduce the lever-arm ratio by the factor $\cos \lambda/(1 - \sin^2 \lambda/d^2)^{1/2}$. Otherwise, the resolved shear stress increases as extension takes place.

The stress was transmitted from the weight pan to the lever arm and from the lever arm to the specimen through steel tapes which followed profiles. The profile on the end of the lever arm attached to the specimen with a 3-inch gage length was circular with a radius of 6 inches from the profile to the knife-edge suspension. Four profiles were made for the other end. Each was calculated to give an initial lever-arm ratio of 2:1 and then decrease according to the factor quoted above for extensions out to 15 percent. One was made for each of the initial angles of λ of 30°, 35°, 40°, and 45°, λ being the angle between the slip direction and the specimen axis. Since face-centered cubic crystals have 12 octahedral slip systems, this range of profiles was suitable for the most favorably oriented slip system in most crystals.

The lever-arm system had to be balanced so that its center of gravity was exactly at the center of rotation, so that no external moments other than the applied one would act after extension began. First, the profiles were made to weigh the same and to have approximately the same moments. Second, a small weight pan was attached to the specimen side of the lever arm for adjusting the moment to zero when the lever arm was in a horizontal position. Third, a threaded shaft was mounted directly above the point of the knife-edge suspension. Two threaded steel plates placed on this shaft enabled a coarse and a fine adjustment to be made, so that the vertical position of the center of gravity of the whole lever-arm arrangement could be adjusted to the line of the knife-edge contact about which rotation takes place. Thus, the lever-arm arrangement remained balanced throughout the whole range of extension for which it was designed.

Capacitance Strain Gages

Two capacitance-type strain gages have been used in this investigation. The one containing flat parallel plates in the pickup has been described in reference 3. This unit has been redesigned slightly, so that now both capacitance plates are mounted on the same shaft. This

increases the stability of the unit, while adding slightly to its weight. Although this unit has a very high sensitivity, the sensitivity is not linear over much of the range. The range can be increased with some sacrifice in sensitivity. Typical values from calibration curves indicate that, for a range of 0.02 inch, the sensitivity varies from 1.6 to 16 microinches per millivolt. For a range of 0.10 inch, the sensitivity varies from 4 to 50 microinches per millivolt. The unit can be rezeroed mechanically to increase the total range.

Because of the larger strains anticipated in these elevated-temperature tests, a new type of capacitance strain gage was developed. The pickup for this unit is a dual-capacitance type with cylindrical plates, as shown in figure 1. It is constructed so that, as extension takes place, the central cylinder moves within the concentrically located rings. Thus, the capacity increases in one section and decreases in the other. The capacitance pickup has a total electrical range of 10 to 50 micromicrofarads per section.

The outer shell and the end plates of this unit are made of Lucite, and the other parts are constructed of commercial 2S aluminum. The center cylinder has four holes drilled through it to reduce its weight. The pickup is connected to the specimen by stainless-steel arms similar to those used with the flat parallel-plate pickup. One end of the specimen is connected to the Lucite case and the other end, to the push rod.

The four parts of the capacitance-measuring unit are shown in figure 2. The oscillator is a push-pull type employing the same tuned circuit for both grid and plate circuits. The variable condenser in this tuned circuit allows the sensitivity to be varied from approximately 10 microinches per millivolt to as low a sensitivity as is desired. The variation in sensitivity has little effect upon the range. The sensitivity is linear within approximately 2 percent over a range of 0.30 inch. A typical calibration curve is shown in figure 3.

The oscillator is inductively coupled to two tuned circuits consisting of L_1, L_2, and the capacitance pickup. By means of discriminator action, the variations in capacitance of the pickup produce a proportional direct-current voltage across the two 100,000-ohm potentiometers at the output of the discriminator. The potentiometers are linear types and are ganged together. This facilitates rezeroing electrically in order to achieve high sensitivity over the entire range.

The output of the discriminator is amplified by the direct-current amplifier and applied to a recording instrument. The two 100-ohm resistors across which the output voltage is developed can be changed to match the input impedance of the recording device. The 1,000-ohm

variable resistor in the cathode circuit of the 6N7GT tube is used to adjust the linearity of the stage. This control remains fixed after it is set initially, unless the tube is replaced. The fourth part of this measuring unit is the power supply.

The lead wire from the measuring unit to the pickup was 300-ohm television cable. However, since stray and lead-wire capacities have a large effect on the sensitivity of the instrument, it was necessary to calibrate the unit with the lead wires in the same position that they would be in during a test. Therefore, the cable was replaced by a 185-ohm shielded twin lead, with the shield used as the ground wire. For short lengths of approximately 2 feet, this wire does not exhibit the above shortcoming. The linear sensitivity and the extended range, which can also be increased by mechanically rezeroing the capacitance pickup, have been found to be extremely useful in this investigation.

EXPERIMENTAL PROCEDURE

Preparation of Crystals

The single crystals of aluminum were grown by the strain-anneal method in the form of tensile specimens with a 3-inch reduced section which had been machined to a 0.505-inch diameter. The method has been discussed at length in references 2 and 3. The crystals were grown primarily from high-purity (99.99+ percent) aluminum containing 17 parts per million of copper, 10 parts per million each of iron and silicon, 6 parts per million of sodium, 3 parts per million of magnesium, and no detectable manganese or calcium. A few crystals were also grown from a slightly lower purity aluminum, approximately 99.95 percent. This material contained 200 parts per million of silicon, 80 parts per million of iron, 50 parts per million of calcium, 30 parts per million each of manganese and magnesium, 8 parts per million of lead, and 5 parts per million of copper. These determinations were made by spectroscopic analysis.

In order to be able to increase the yield of large single crystals from the growth process, the amount of prestraining was varied to determine more accurately the critical value of the amount of prestraining. From the summary of the results of the two growths of 54 specimens each presented in table 1, it appears that 1- to $1\frac{1}{4}$- percent prestrain yields the maximum number of crystals throughout the entire 3-inch reduced section for the high-purity aluminum. Since a total of only 12 of the lower purity crystals was grown, the prestrain was not varied for these specimens. However, the critical amount of prestraining increases as

the purity decreases. This prestraining follows a 6-hour anneal at 550° C for grain-size stabilization and precedes the final anneal, which takes 11 days, starting at 450° C and ending at 635° to 640° C.

After the crystals were grown, they were etched with a solution containing 50 parts hydrochloric acid, 48 parts nitric acid, and 2 parts hydrofluoric acid by volume. For the most part, the specimens were electropolished according to the procedure mentioned in the section "Electron-Microscope Techniques."

The orientation of each specimen, or the largest crystal in the gage length, was determined by the Laue back-reflection X-ray technique. The orientations of the cube faces and the most probable slip systems are presented in table 2. The crystals have been grouped according to their use, although some crystals have been used for more than one test or observation. The angles α, β, and χ are the angles the three cube planes make with the specimen axis. The angle between the slip direction and the specimen axis is given as λ, and the angle between the normal to the slip plane and the specimen axis is given as ϕ. With but one exception, crystal S-64, the orientations of the slip planes reported are the three most favorable (111) types of planes. These are tabulated along with the values of λ for the associated [110] directions and the values of $\cos \phi \cos \lambda$. This is true for all but the last section of table 2, "Crystals for constant-load creep tests." In these specimens other slip planes have been important, so the reported plane may be a (111), (100), or (211), but the associated slip direction is still a [110] direction.

Testing Procedure

In the constant-load-rate tests, the load rate was held approximately constant throughout the test at a value between 1/2 pound per minute and 2 pounds per minute. This load rate could be varied by varying the power input to the vibrator which moved shot along a trough and into a container on the weight pan. This load was applied on the long portion of a lever arm with an arm ratio of 9:1. A spring scale was placed in the linkage between the lever arm and the weight pan for load measurements. The test was started after the lever-arm assembly had been balanced to give no net load on the specimen. A 2-inch gage length was used in these tests.

In the creep tests the loading was accomplished by releasing a hydraulic jack holding the weight pan. As a matter of technique, a 50-pound weight was placed between the weight pan and the jack to insure that the jack would release the load freely but without impact. The recording apparatus for the capacitance strain gage allowed the entire creep curve to be recorded continuously and automatically. In the

constant-stress tests, the entire system was balanced with the specimen and capacitance strain gage in place. Then the weight pan and any additional weights would act as the applied load. In these constant-stress tests, a 3-inch gage length was employed, and only specimens with a single crystal throughout the entire 3-inch reduced section were used. The arms from the capacitance strain gage were attached to the shoulders of the specimen.

In the prestrain experiments, two different types of prestraining were employed. A rapid strain rate was obtained by dead-weight loading or essentially rapid initial elongation. A relatively slower strain rate was obtained in a constant-load-rate test. Since the initial extension could not be predicted reliably, this prestraining by dead-weight loading was carried out first on one specimen. Then prestraining in a constant-load-rate test could be carried out to the same shear strain on a second crystal, so that the effects of the two types of prestraining could be compared on the basis of the same shear strain.

In the prestraining operation, the extensometer was connected to the specimen on its shoulders. This prevented any damage resulting from the contact between the knife edges and the crystal in the 2-inch gage length used in the subsequent test. Specimens for which test results were to be compared directly were chosen to have approximately the same values of $\cos \phi \cos \lambda$, the factor which determines the fraction of the tensile stress which is resolved in the slip plane in the slip direction. When the prestraining was performed at elevated temperatures, a split furnace was used so that the furnace could be removed shortly after the prestraining operation had been completed. In the subsequent test upon which the effect of prestraining was being studied, an attempt was made to minimize and to equalize the heating periods. This tended to reduce and to standardize any recovery effects which may have been important at the temperature of the test.

X-Ray Diffraction Methods

A normal back-reflection Laue technique has been employed for the determination of crystal orientations. This method has been useful also for the determination of the operative slip plane in elevated-temperature tests. When the slip bands on a deformed crystal exhibited abnormally large shear strains, a back-reflection Laue photograph was taken normal to the shelf produced by the slip band. In this manner the operation of slip systems containing the (100) and the (211) slip planes was confirmed. However, the resolution of this technique is not sufficient to detect tensile strains less than about 2 percent, so it was necessary to use techniques with higher resolution to detect and to follow the strain throughout the various stages of a prestrain experiment.

The first of these techniques to be used was the "oblique Laue" method. The experimental arrangement for this method is presented in figure 4. An arrangement of two rectangular slits, each with one very small dimension in the vertical direction, was used to limit the area of the crystal to be photographed. Specimens studied by this method were crystals with a (100) plane nearly parallel to the crystal surface. With the arrangement of figure 4, each Laue spot from a perfect crystal is elongated into a streak composed of a continuous-radiation spectrum over the spectral range permitted by the geometrical divergence of the slits. With an imperfect crystal, the spectral band would be lengthened, but the sensitivity with respect to local orientation changes would not be very high. To improve the sensitivity, the angle of incidence of the X-ray beam upon the crystal was adjusted to superimpose the characteristic L-beta spectrum, from the second order of the (100) plane, upon the continuous-radiation streak. Different wavelengths are reflected from different parts of the irradiated area of the crystal at their respective Bragg angles. The ability of the crystal to resolve the individual lines in the tungsten L-beta spectrum gives a good indication of the regularity or perfection of the crystal lattice in the small region being photographed. In this method a single reflection is studied in detail before deformation, after prestraining, and then after a creep test.

The second method to be used was an X-ray reflection micrograph method. The experimental arrangement for this technique is presented in figure 5. Unfiltered copper radiation was employed. The crystal was oriented with the aid of a portable Geiger tube, so that the K-alpha wavelength was reflected by the (200) planes, which were approximately parallel to the crystal surface. A slit-formed beam, well collimated in its short horizontal dimension, was reflected from the crystal. Because of the large distance between the X-ray source and the slits, some effective collimation was achieved in the long vertical dimension. The photographic plate and the crystal were translated without any relative motion between the two, in order that a larger area of the crystal could be examined. The translation extended the line image of the beam, defined by the slits, into a band. If the crystal were perfect, the band would be of uniform intensity. Any gross crystal imperfections would result in intensity deficiencies in the image. Hence, an X-ray micrograph of the lattice distortion was obtained. The high resolution of this method is a result of the large target-to-crystal distance (31 centimeters), the short crystal-to-plate distance (approximately 1 to 2 millimeters), and the fine slits (reference 5). Exposures were made on either lantern slide or Type V-O photographic plates.

All exposures have been made with the X-ray tube operating at 10-milliampere current and a voltage of approximately 35 kilovolts.

Electron-Microscope Techniques

Present-day electron microscopes require specimens thin enough to be permeable to an electron beam. Therefore, metal surfaces must be studied by means of replicas. Anodic-oxide replicas can be made from aluminum and aluminum alloys. The technique has been described by several investigators (refs. 6 and 7). Anodic-oxide replicas were used in the initial stages of this investigation. They were quite strong and held up well in the electron beam. Some difficulty was experienced in obtaining replicas of uniform thickness. Also, the replicas were quite likely to be dirty. Neither of these factors is too serious if the samples are easy to prepare, so that several sets of replicas can be prepared under varying conditions of anodization. However, it was not practicable to prepare a large number of creep specimens for electron microscopy. Therefore, a major portion of the effort in this investigation was devoted to developing a replica technique which would not destroy the creep specimen, thus making it possible to prepare several sets of replicas from one specimen.

The practicability of a specific replica technique depends on the nature of the surface to be replicated. The surface of the aluminum bars had to be prepared so that fine structure in the slip bands after creep could be observed. During most of the investigation electropolishing, in a bath consisting of equal parts by volume of methanol alcohol and concentrated nitric acid, followed by etching in a modified aqua regia solution appeared to be the best surface preparation.

The polished specimen surface was protected against oxidation during testing at elevated temperatures by one of two methods. One method was to perform the test in vacuum; the second was to coat the specimen with Dow Corning 710, a silicone oil. This was possible for temperatures up to 500° F or slightly higher. After testing, the oil could be dissolved in xylene.

The replica techniques, other than the oxide replicas, involved stripping a thick, plastic film from the aluminum bar. If this initial plastic was Zapon, then a positive plastic replica could be made by flowing Formvar on the surface of the Zapon. The Zapon was then dissolved in amyl acetate, leaving the Formvar, insoluble in amyl acetate, in the form of a positive replica. This technique has been described in detail elsewhere (refs. 8 and 9). However, these plastic replicas did not hold up well over the etch pits or over sharp corners in the slipped regions.

A method for preparing multiple aluminum oxide replicas from a single surface has been described by Hunter (ref. 10). He evaporated a thin film of aluminum on a stripped plastic replica. He then formed an oxide layer on the outer surface in an anodizing bath and dissolved away the aluminum

and the plastic, leaving the oxide replica. It was felt that, for the purposes of this investigation, the surface of the aluminum adjacent to the plastic replica would have to be anodized. Several methods for separating the aluminum film from the plastic and then anodizing the inner surface were tried without much success. This technique is potentially good if some method can be devised for separating the soft aluminum film intact from the plastic.

During the latter part of the investigation, the formula for Alcoa R5 Bright Dip, a patented chemical polishing treatment licensed by Aluminum Company of America, was obtained. This chemical polish was followed by an etch of a few seconds' duration in a solution containing 10 cubic centimeters of concentrated hydrochloric acid, 30 cubic centimeters of concentrated nitric acid, and 20 cubic centimeters of a 5-percent ferric chloride solution to develop etch pits. The faces of etch pits developed by this solution represent (100) planes. With this surface preparation it was possible to make replicas consisting of a thin, evaporated, platinum film backed by an evaporated silica film. These replicas held up quite well over the small etch pits developed by the ferric chloride etch. As a result of the thinness of the platinum film and the large scattering cross section of platinum atoms for high-energy electrons, the contrast was sufficient to disclose fine structure in the slip bands.

This platinum-replica technique was developed at Battelle. The method was applied as follows: A strip of Faxfilm, wet on one side with acetone, was pressed onto the aluminum bar and then stripped when dry. Platinum was evaporated from two sources on opposite sides of the film and inclined at 45° angles to the film. One source was about double the strength of the other, to give shadow contrast. Then silica was evaporated at normal incidence. The platinum-silica-coated plastic was cut into small squares. The squares were placed on specimen screens, and these, in turn, were placed on a coarse-mesh screen in a glass container. Acetone was added barely to cover the coarse screen. After two or three changes of solvent, the plastic was dissolved and the replicas were ready for viewing in the microscope.

Faxfilm strippings have also been used to replicate the surfaces of these round aluminum single crystals for light microscopy. This produces a flat replica from a curved surface that ordinarily would be difficult to reproduce in a micrograph. The strippings can be used directly as replicas, or they can be shadowed with metal for better contrast.

EXPERIMENTAL RESULTS AND DISCUSSION

Stress-Strain Curve

Prior results (ref. 2) had shown that the critical resolved shear stress at room temperature increased by almost an order of magnitude when the purity was decreased from 99.99+ to 99.95 percent. Previous work (ref. 3) had also shown the stress-strain curve to be quite dependent on the test temperature. Therefore, stress-strain curves were determined in constant-load-rate tests at 82°, 500°, and 1,100° F for each of two purities, 99.99+ and 99.95 percent aluminum. These stress-strain curves were determined primarily to compare the effect of temperature and the effect of impurity content on the plastic properties of single crystals of aluminum over the range of temperature of interest. These stress-strain curves are presented in figure 6, along with two curves reported by Boas and Schmid (ref. 11) at temperatures of 64° and 1,112° F for aluminum single crystals of 99.63-percent purity containing predominantly 0.23 percent iron and 0.14 percent silicon.

The data (stress σ versus strain ϵ) from these tests were converted to shear stress τ and shear strain γ and corrected for the rotation of the slip direction toward the tension axis during extension. For values of tensile strain less than 1 percent, the resolved shear stress is given within 1 percent by the equation:

$$\tau = \sigma \cos \phi \cos \lambda \tag{1}$$

With larger strains the resolved shear stress varies during extension according to the following equation (ref. 4):

$$\tau = \sigma \cos \phi \left(1 - \frac{\sin^2 \lambda}{d^2}\right)^{1/2} \tag{2}$$

For tensile strains of 1 percent or less the resolved shear strain is given within 1 percent by the relation:

$$\gamma = \epsilon / \cos \phi \cos \lambda \tag{3}$$

For larger strains the resolved shear strain is also affected by the lattice rotation. The shear strain has been described analytically in terms of the original orientation and the tensile strain ($d = 1 + \epsilon$) by Schmid and Boas (ref. 12) with the relation:

$$\gamma = \frac{1}{\cos \phi}\left[\left(d^2 - \sin^2 \lambda\right)^{1/2} - \cos \lambda\right] \tag{4}$$

A decrease in purity from 99.99+ to 99.95 percent has caused an increase in the stress required to produce a given strain. This increase in stress varies from approximately 40 to 85 percent for the curve at 82° F over the range of shear strain from 0.04 to 0.20. For the two curves at 500° F over a similar range of strains, the increase varies from 150 to 80 percent. For the two curves at 1,100° F, the increase varies from 50 percent to almost 0 percent over the same range of strains.

Concerning the magnitude of this increase produced by a small decrease in purity, the increase is quite important at 82° F and 500° F but becomes almost insignificant at 1,100° F. The effect of a still further decrease in purity to 99.63 percent is demonstrated by the curves reported by Boas and Schmid at 64° F and 1,112° F. Although the increase in the stress level at 64° F is appreciable, the important fact is that the stress level has been raised considerably at 1,112° F. Although not readily apparent from these curves, there is a large effect of the impurity content on the yield stress or the critical resolved shear stress, that is, the stress that marks the initiation of plastic deformation.

To observe the effect of temperature on the stress-strain curve, one need only to pick out the curves designated by the same type of line. When these data were plotted on logarithmic paper, a fairly linear range existed in the plots over the range of strains from 0.05 to 0.20 or more. The slopes of these curves are referred to ordinarily as the strain-hardening coefficients. Although the slopes decreased with increasing temperature for the 99.95-percent-pure crystals, no similar trend was apparent in the case of the 99.99+-percent-pure crystals. Therefore, no comparison of the effect of impurities on the strain-hardening coefficient as a function of temperature could be made.

These tests have been extremely useful in obtaining information on the flow stress required to produce a given strain in these aluminum single crystals at various temperatures. They have also given a good indication of the effect of alloying elements on the mechanical properties that might be expected with small amounts of alloying additions in elevated-temperature tests.

Because the processes or mechanisms of slip, kinking, and polygonization are present in the total deformation process, it is felt that the effects of temperature and impurity content on the stress-strain curve are related directly to the manner in which these two variables affect the movement and generation of dislocations. However, this relationship is probably not a simple one. In this respect, Cottrell has discussed the effect of solute atoms on the behavior of dislocations (ref. 13). The primary effect of the solute or impurity atoms is to retard the movement of dislocations through the interaction of the stress fields

associated with the solute atoms and the dislocations. An increase in temperature enhances the deformation process by increasing the internal thermal energy and thermal fluctuations, increasing the amplitude of vibration of the atoms, and decreasing the bonding energy between atoms. This eventually results in propagation of slip on planes other than the close-packed octahedral planes at elevated temperatures.

Work-hardening was first attributed to the interaction of dislocations by Taylor (ref. 14), who pointed out that dislocations exert forces on one another. Koehler has discussed the nature of work-hardening on the basis of interaction-hardening (ref. 15), which predominates at high strains, and on the basis of source-hardening (ref. 16), which predominates at low strains. The sources referred to are the so-called Frank-Read sources (ref. 17), which have been postulated by Frank and Read to explain the multiplication of dislocations during plastic deformation and to account for the occurrence of avalanches of slip on one plane. These sources are stopped when some dislocations become blocked at barriers and a back stress builds up.

In general, the initiation of plastic deformation is better understood than these later states of deformation involving work-hardening. The yield phenomenon in single-crystal and polycrystalline metals has been discussed by Cottrell (ref. 18). He attributed the yield point to the release of anchored dislocations. This takes place when the summation of the external or applied stress and any internal stresses, enhanced by thermal fluctuations, is sufficient to free the first anchored dislocations. Plastic deformation is not observed until these moving dislocations receive enough energy to surmount the barriers presented by the mosaic boundaries and other obstacles present in the metal, in order that slip can propagate through the bulk of the metal.

Creep Curve

The data from the constant-stress creep tests at elevated temperatures are presented in linear-coordinate plots of total shear strain versus time in figures 7 through 10. These data are presented in a summarized form in logarithmic plots in figure 11. Crystals used in these tests were specimens which contained a single crystal throughout the entire 3-inch reduced section. They had no favorably oriented high-temperature slip systems which might operate at the temperature of the test. This was necessary so that the operative slip system would be the one containing the (111) plane and the [110] direction with the highest resolved shear stress. By determining the operative slip system prior to testing, the correct profile could be chosen to maintain an approximately constant resolved shear stress throughout the test. The tensile strains have been converted to shear strains by

equation (3) for the strain-time plots presented. The creep curves have all been drawn on the same scale for easier visual comparison of the curves in various figures.

Prior to performing these elevated-temperature tests, it was necessary to determine whether an oxide layer might affect the reliability of the creep measurements. An oxide layer was formed on one crystal by anodizing at 70 volts and on another by annealing in air for 1 hour at 1,000° F. In neither case was any appreciable effect observed on the creep properties of these high-purity single crystals when tested at 300° F and 400-psi resolved shear stress. However, the result might be expected with single-crystal specimens 1/2 inch in diameter, since most experiments designed to study the effect of oxide layers employ much smaller specimens. In smaller specimens the cross-sectional area of the oxide layer itself may be an appreciable fraction of the cross-sectional area of the specimen. Because of this result, it was not considered necessary to build vacuum-creep units to obtain reliable creep data at elevated temperatures.

The effect of the impurity content on the plastic properties, as detected in the stress-strain curves, has been checked also on the creep curve from two specimens deformed in vacuum at 500° F for electron-microscopy observations. Specimen S-20 extended 12.4 percent in 25 hours at 300-psi resolved shear stress, as compared with a resolved shear stress of 970 psi (more than three times as large) which was necessary to extend crystal L-12 12.4 percent in 17 hours, both in constant-load creep tests.

The maximum strain for the highest stress at each temperature in the constant-stress tests has been limited by the range over which the profiles were designed to maintain a constant resolved shear stress. The range of temperatures investigated was from 400° to 900° F. In this range of temperatures recovery was definitely an important factor, although recrystallization was not observed, probably because the crystals were not sufficiently highly deformed.

Creep curves for three stresses at 500° F are shown in figure 7. These curves are similar to those obtained in the temperature range from room temperature to 400° F (ref. 3). They exhibit a continually decreasing slope. Although the slope appears to reach a constant value, which might be termed the steady-state or minimum creep rate, the magnitude of this slope depends on the time scale chosen. This can be demonstrated by plotting the data on two time scales, one in units of seconds and the other in units of hours. Both plots will tend toward an approximately constant slope. However, the magnitudes of the slopes from the two time scales differ considerably, the slope from the plot with the second scale being approximately equal to the initial slope of the curve on the hour scale. This characteristic type of creep curve

was observed also at the lowest stress, 50 psi, at 700° F (see fig. 8) and at 400 psi at 400° F (see fig. 10). A creep rate that continually decreases may be detected by plotting the creep curve logarithmically, as in figure 11. On such a plot, the slope of the line will be less than unity and will never increase, although a decrease in slope is possible. This type of curve, exhibiting a continually decreasing creep rate, has been observed also by Hazlett and Parker (ref. 19).

The remainder of the constant-stress creep curves from figures 8, 9, and 10 appear in figure 11 as curves which are convex downward, rather than straight lines. The reason for this curved plot has been the point of considerable controversy, as evidenced by the recent discussion by Roberts and Grant of Hazlett and Parker's ideas (ref. 19). References have been quoted to back up both viewpoints. The viewpoint of Hazlett and Parker has been supported by the results of an independent investigation by Bhattacharya, Congreve, and Thompson (ref. 20). Likewise, Roberts is backed up by the bulk of the work by Andrade (ref. 21) and the more recent work of Cottrell and Aytekin (ref. 4).

Hazlett and Parker preferred to interpret this curvature to be a result of the time-independent strain occurring in the initial extension. They claimed that the initial extension should be subtracted from the total strain prior to plotting the data, in which case the logarithmic plot again assumed its linearity. This assumption appears to be reasonable since one would not expect that the initial extension would follow a relation involving the time. This method of plotting was tried on the data from several of the constant-stress creep tests in this investigation without complete success. An amount of strain usually could be found which, if subtracted from the total strain, would result in a linear logarithmic plot. However, this amount of strain was generally larger than the observed initial shear strain in the creep tests. This was especially true at the higher temperatures. Since much lower stresses had to be used at the higher temperatures to obtain comparable curves, the initial shear strains were correspondingly less. Hence, if the observed initial shear strain was subtracted from the total shear strain prior to plotting, many of the curves were still convex downward. The amount of curvature is more than can be accounted for by the fact that the shear strains were not corrected for rotation by equation (4). Therefore, unless the stress was not truly constant, it appears that the curvature in some of these logarithmic plots must be due to a decrease in the rate at which the creep rate is decreasing, if not to an approximately constant creep rate.

Concerning the characteristic creep curves presented in figure 11, some generalizations can be made. The linear plots are predominant at high stresses and low temperatures, whereas the plots which are convex

downward are predominant at lower stresses and higher temperatures. These results are in agreement with the recent work of Roberts (ref. 22), who studied the creep behavior of extruded electrolytic magnesium in polycrystalline form. The two curves which are convex upward (100-psi resolved shear stress at 500° F and 50-psi resolved shear stress at 700° F) are, in both cases, for the lowest stress investigated at each temperature. The lowering of the first portion of the curve may have resulted from a small amount of accidental prestraining prior to testing. However, this strain should have been annealed out before the load was applied. On the other hand, the lowering of the later portion of the curve may have resulted from the onset of duplex slip, which is known to retard the creep process (ref. 3). In this investigation duplex slip has also been observed on a fine scale in the slip bands on crystals deformed during creep at elevated temperatures. It might also have resulted from the retarding effect of kink bands on the slip process, since slip bands have been observed to stop in the kink bands in this investigation. In the 900° F tests, the 25-psi and 40-psi tests were performed with the same crystal. This crystal was annealed for 1/2 hour at 900° F with the load removed after a shear strain of less than 1 percent in the 25-psi test.

Many investigators have employed various methods for analyzing and correlating creep data in empirical or mathematical forms in addition to those already mentioned. Wyatt (ref. 23) has analyzed transient creep in pure metals, and Cottrell (ref. 24) had discussed several of the time laws of creep. Sherby and Dorn (ref. 25) have correlated the creep data from alpha solid solutions of aluminum, and Johnson and Frost (refs. 26 and 27) have discussed the application of various relations to creep data from elevated-temperature tests. Most of these methods employ more than one empirical constant, and usually three constants, to describe the time dependence of the creep process. The few theoretical attempts to describe creep have been discussed in references 1 and 3.

In the work reported here it has not been possible to describe accurately the time dependence of the results of the constant-stress creep tests summarized in figure 11 in a simple manner. Therefore, a complete mathematical analysis of the stress and temperature dependences of the creep process has not been obtained. It is felt that these results are indicative of the complex nature and the differing kinetics of the processes which make up the total deformation process, even in the case of creep of single crystals of high-purity aluminum. From a study of the inhomogeneity in creep deformation of coarse-grained high-purity aluminum, Chang and Grant (ref. 28) have concluded that any mathematical description of the creep curve must be considered to be a statistical summation of the equations describing the various component processes of creep. Since three mechanisms of deformation have been observed in this investigation, it is felt that the description and understanding of these basic mechanisms are more important than developing an empirical relationship which

may describe the creep process mathematically without any physical insight regarding the creep process itself. Naturally, both would be desirable if they could be obtained.

Prestrain Experiments

Relatively little work has been reported on the effect of prestrain on creep, or, for that matter, any other type of plastic deformation. Probably the most complete investigation of this type has been reported by Kennedy (ref. 29), who studied the effect of instantaneous prestraining (of the order of 5 seconds) on constant-stress creep in polycrystalline lead. He investigated the effect of prestrains from 0 to 16 percent at temperatures of 100° C, 35° C, and -180° C on the creep curve at room temperature at three stress levels out to a total time of 3 hours. He fitted the resulting data to Andrade's law, involving two arbitrary constants β and k, by shifting the time scale of the strain-time plot. In this work he found that the amount the time scale had to be shifted increased with increasing amounts of prestrain and decreased with increasing temperature of the prestrain. For prestrains up to 10 percent the creep curve from a prestrained specimen could be made to coincide with the curve from an unstrained or control specimen by this shift in the time scale. However, for prestrains larger than 10 percent a decrease in one of the arbitrary constants k was necessary.

Bhattacharya and coworkers (ref. 20) have studied the effect of prior strain on creep of polycrystalline aluminum at 150° C under a constant tensile stress. As mentioned previously, they found that the creep strain (the total strain minus the initial strain upon loading) followed a power-law relationship with time, defined by two constants, a coefficient a and an exponent k for the time parameter. In a rather sketchy analysis, they found that the constant k increased and the constant a divided by the seventh power of the applied stress decreased with increasing prestrain out to 6 percent and that both were approximately constant with larger amounts of prestrain. The constant a was divided by the seventh power of the applied stress since the stress had to be raised to obtain similar rates of creep as the degree of prestrain was increased. The only points that the authors noted concerning these results were that the power-law relationship still existed for the prestrained specimens and that very small amounts of prior strain could well account for the unsatisfactory reproducibility often observed in the creep behavior of pure metals.

Other viewpoints have also been expressed on the effect of strain rate and temperature on plastic deformation. Brown (ref. 30) attempted to describe qualitatively an equation of state to explain the effects of a change in the temperature or in the strain rate during a tensile test; that is, a faster strain rate or a lower test temperature produced a higher stress-strain curve. Rosi and Mathewson (ref. 31) observed this effect of changing the temperature on the stress-strain curve of single

crystals of high-purity aluminum at low strains up to 1-percent extension. Ellis and Greiner (ref. 32) found that the effect of decreasing the rolling temperature was to raise the stress-strain curve (i.e., increased flow strength and ultimate strength) at room temperature. They concluded that this observed effect was caused by simultaneous recovery during the rolling operation.

Following this brief review of the limited amount of material available on the effect of prestraining, the results of this investigation, presented in figures 12 through 16, will now be discussed. The effects of prestraining to the same shear strain by a very rapid strain rate and by a comparatively slower strain rate on the room-temperature stress-strain curve are depicted in figure 12, along with the stress-strain curve from a control, or unstrained, specimen. The amount and the path of the prestrain have been included in both plots, so that the total shear strain and the resolved shear stress could be corrected for rotation. The two crystals that were prestrained had almost identical orientations. Still, only about two-thirds of the stress required in the rapid prestraining by dead-weight loading was required to produce the same shear strain in the slow prestraining in a constant-load-rate test. It was perhaps significant that no strain was detected in the subsequent constant-load-rate tests below the stress level to which the crystals had been prestrained. Therefore, no appreciable recovery had taken place at room temperature during the period of approximately 24 hours which elapsed between the time the crystals were prestrained and the time the stress-strain curves were obtained. The most important consequence of the prestraining was to increase the yield stress of the crystals. For comparable amounts of shear strain the rapid prestraining was more effective than the slow prestraining in raising the stress-strain curve.

The effect of increasing the amount of rapid prestraining at room temperature on the creep curve at 200° F and 400-psi resolved shear stress is shown in figure 13. The prestraining decreased the initial shear strain substantially. However, at this temperature strain-hardening was very predominant. Therefore, it was difficult to determine the effect of the prestraining on the later stages of creep, since the creep rate decreased rapidly even in the unstrained control specimen. An increase in the amount of the prestrain increased the observed effect; that is, the decrease in the initial shear strain and the lowering of the creep curve were more pronounced. In these and subsequent curves the amount of the prestrain has not been included in the total shear strain.

The result of varying the temperature of the rapid prestraining and its effect on the creep curve at 300° F and 300-psi resolved shear stress are presented in figure 14. Increasing the temperature of the prestraining from room temperature to the testing temperature reduced the effect of the prestrain considerably. The effect of the prestraining at the elevated temperature was less for a larger amount of prestrain, although

the stress required to produce this larger strain was slightly lower. Again, the primary effect of the prestrain was to reduce the initial shear strain and to lower the total shear strain and the level of the creep curve.

The effects of both rapid and slow prestraining at room temperature on the creep curve at 300° F and 400-psi resolved shear stress are shown in figure 15, along with a control curve from an unstrained crystal. Similar plots for both types of prestraining performed at 300° F to a larger shear strain are presented in figure 16. In addition to reducing the initial shear strain, the creep rate in the later stages of the creep process also was reduced. In prestraining at 300° F, the faster strain rate was more effective in enhancing the creep resistance of the single crystals. Although this trend was also observed in the stress-strain curves (see fig. 12), it was not observed with the room-temperature prestraining in figure 15. This may have resulted from some accidental prestraining of the crystal, S-94, in addition to the intentional slow prestraining. The crystals were extremely soft, and this particular crystal had to be handled more than most because of the X-ray pictures taken before and after prestraining and after the subsequent creep test.

Although not without exception, the effect of prior strain on the creep curve can be described. As determined in this investigation, the effect of prestraining is to reduce the initial shear strain considerably, to remove a portion of the early or transient portion of the creep curve, and, in some instances, to reduce the creep rate in the later stage of creep. The larger the amount of the prestrain, the more the shape of the creep curve is affected. Also, increasing the temperature of the prestrain reduces its influence on the creep process. The most important observation that has been made is that the rapid prestraining obtained in dead-weight loading is more effective in hardening the crystals and increasing their resistance to plastic deformation than the slower prestraining obtained in a constant-load-rate method of deformation. Since the resolved shear stress required to produce the same shear strain is higher for the rapid prestraining than for the slower prestraining, dislocation theory provides a reasonable explanation for this behavior. The higher stress level involved in the rapid prestraining has used up more of the Frank-Read sources than were present in the crystal initially. The stress required to operate a Frank-Read source is Gb/l, where G is the shear modulus, b is the Burgers vector or unit slip distance in the slip direction, and l is the length of the source (ref. 33). Thus, the longest sources operate at the lowest stress level. Since a larger applied stress is required in the rapid prestraining to produce the same shear strain as that produced with the relatively slower prestraining, the sources would be effectively used up to a higher stress level by the rapid prestraining. The resulting increases in hardening of the crystals can be attributed to source-hardening, as defined by

Koehler (ref. 16) in his analysis of stress-strain data at low strains.

The concept that more Frank-Read sources and, hence, more active slip planes are operative with the faster strain rate is consistent with the fact that the deformation is more uniform with the faster strain rate. This same observation has been made on crystals deformed at two relatively different strain rates at 1,100° F. Hence, the process of slip-band formation is related directly to the strain rate. This will be discussed further in a later section covering the observations of slip bands by light microscopy.

The above description of the effect of prestraining on the creep behavior of single crystals of aluminum has been stated in terms of trends purposely because of the difficulty encountered in obtaining reproducible results. This difficulty is due in part to the almost unavoidable amount of accidental prestraining which occurs during handling of these soft crystals, in part to the fact that the crystals do not have identical orientations, and in part to the inherent microscopic differences in the single crystals even in the annealed state. Regarding the latter cause, Parker and coworkers (ref. 34) have found that the yield stresses of zinc single crystals with identical orientations can be more than doubled by varying the annealing procedure prior to testing. They associate this result with the effect of subboundaries existing in the zinc crystals. The status of these subboundaries, which apparently can be changed by the annealing procedure, must play an important part in determining the plastic properties of metals. A fine substructure of the order of 1 micron in linear dimensions has been detected in this investigation in the annealed aluminum single crystals. Therefore, it is apparent that the effect of annealing procedure and deformation of this substructure will have to be understood before further experiments on the effect of prestraining are undertaken.

X-Ray Diffraction Investigation

High-resolution X-ray diffraction techniques have been employed to obtain an indication of crystal perfection and to study the changes produced in the crystalline lattice by small amounts of prestraining and by subsequent deformation in creep. Since the oblique Laue technique was not a conventional one, photographs have been made by three methods from a crystal found to be imperfect after the growth process. The imperfect nature of the crystal was noticed first in the normal back-reflection Laue photograph in figure 17(a) used for the determination of the crystal orientation. This photograph was made with the standard specimen-to-film distance of 3 centimeters and ordinary pinhole collimators with continuous tungsten radiation. When the large pinhole collimators were replaced by a collimating system consisting of a fine pinhole

(150 microns in diameter) and a fine slit (3 millimeters by 150 microns), the photograph shown in figure 17(b) was obtained. The use of the fine collimators increased the resolution and the detail observable in the individual reflections, although with the considerable increase in the required exposure time from 10 minutes to 12 hours.

A still further increase in resolution was obtained by observing the reflection of the tungsten L-beta spectrum of a single crystallographic plane with an increased specimen-to-film distance and the collimating arrangement for oblique Laue photographs, as shown in figure 4. A photograph of this type for the (200) planes of this same imperfect crystal is shown in figure 17(c), and a comparison photograph of a relatively perfect single crystal, in figure 17(d). The imperfect crystal exhibited fairly large differences in orientation in both the vertical and the horizontal directions in the area photographed, in addition to not being able to resolve the tungsten L-beta spectrum. However, the relatively perfect crystal, S-13, definitely resolved the individual lines in the tungsten L-beta spectrum. From a comparison of the photographs obtained in the three methods of photographing an imperfect crystal made up of regions of different orientations, one can visualize better what has taken place in deformed crystals which were originally relatively perfect, as indicated by an oblique Laue photograph such as that shown in figure 17(d).

The theory of this oblique Laue method has been mentioned already under "Experimental Procedure." If the sample is a perfect crystal and is alined properly, all the various tungsten L-beta wavelengths will be reflected from the same family of crystallographic planes, but at different positions along the length of the crystal. These characteristic reflections will strike the film at known consecutive positions along the film. As a matter of fact, from the relative intensities and the separations in the photograph in figure 17(d), the various reflections can be identified as the L-beta-4, L-beta-6, L-beta-1, L-beta-3, and L-beta-2 wavelengths, respectively, from left to right. If a fine-grained polycrystalline sample were to be examined, each wavelength would reflect continuously over a considerable portion of the reflection band. On the other hand, if the crystal were composed of crystallites having small disorientations from the average, not all the rays of any one wavelength would strike at the same position along the band. Hence, the relative intensities of the spots would be different from those of a perfect crystal, and the spots might not appear at the correct positions. The amount of disturbance of the oblique Laue photograph from the ideal condition yields a qualitative measure of the imperfections in the area photographed. The interpretation of asterism as being due to distortion or internal lattice strains and of discrete spots as being due to different orientations is the same as in normal back-reflection Laue photographs.

A series of oblique Laue photographs was taken from crystal S-5, initially, after rapid prestraining, and after a creep test at 300° F and 400-psi resolved shear stress. These photographs, shown in figures 18(a), 18(b), and 18(c), show the decreasing ability of the crystal to resolve the different wavelengths after successive deformations. A decrease in reflected intensity is also apparent from a consideration of exposure times. Figure 18(b), taken after prestraining, shows considerable distortion of the original pattern, although no discrete spots were found. This indicates that the lattice was strained, but no new crystallites had formed that could be detected. No difference in this reflection (i.e., no recovery) could be detected in a second photograph after 72 hours at room temperature. Figure 18(c) shows very definitely the presence of many small crystallites, or the formation of a substructure. However, this crystal was found to be bent slightly during the course of this series of photographs and extensions. In addition, the failure of a temperature controller overnight allowed the test temperature to increase from 300° to 575° F, and the crystal extended until the weight pan came to rest on the jack used in loading, after which the crystal remained at temperature with essentially no applied stress. Because of these varying conditions, another experiment was performed.

To increase the resolution of the arrangement shown in figure 4, the 150-micron slit was replaced by a 150-micron pinhole. This necessitated an increase in exposure times by a factor of 10 but increased the sharpness of the reflections. A similar series of photographs was then made on crystal S-8, initially, after a rapid prestraining, and after a creep test at 300° F and 400-psi resolved shear stress. The resolution of this set of photographs, shown in figures 18(d), 18(e), and 18(f), was better, but the results are essentially the same. The initial status of the crystal was very good, as evidenced by the resolution of the five lines in the tungsten L-beta spectrum. The apparent difference in the lengths of the tungsten L-beta spectrum, as shown in figure 17(d) and figure 18(d), was a result of the fact that the crystal surfaces were at different angles with the incident beam. Again, the prestraining introduced considerable distortion, as evidenced by the broadening of the characteristic reflections, but no new orientations were detected. After the subsequent creep test, many discrete spots were evident. However, the discrete reflections were larger than those obtained from crystal S-5 after creep. It appeared that some of the crystallites may have been large enough to reflect all or at least parts of the characteristic tungsten radiation from the L-beta spectrum.

The second high-resolution X-ray technique employed to detect and to follow the strain throughout the course of a prestrain experiment was the reflection-micrograph method. The experimental arrangement for this method is presented in figure 5. Although the method itself has been described by Honeycombe (ref. 5), the translational oscillation of the

film and the specimen to increase the area under observation with this technique is believed to be new. However, this method does increase the exposure time considerably above that required with a stationary specimen. If a single crystal is properly oriented in this beam, a reflection of characteristic radiation will be obtained. Areas of either great or small disorientation in the crystal will not reflect. If the reflection is a low-order reflection, differences in intensity in the reflection may occur as a result of differences in extinction over the irradiated surface of the crystal. However, extinction would not be expected to produce sharp discontinuities in intensity. If the crystal is oriented so as to reflect the continuous radiation, differences in extinction may be observed, but small disorientations will not be observed.

The X-ray micrographs obtained from crystal S-94 initially, after a slow prestrain at room temperature, and after a creep test at 300° F and 400-psi resolved shear stress are presented in figure 19. The specimen was cross scratched to mark the area to be irradiated. The vertical and possibly the horizontal scratches can be seen in figure 19(a), whereas the horizontal scratch shows up well in figure 19(b). The original micrograph of the crystal before any deformation (fig. 19(a)) showed no extra detail when examined at 100X. The continuous variations in intensity can be interpreted as differences in extinction. However, an attempt to correlate these variations with optically apparent irregularities in the electropolished surface of the crystal was not successful. In figure 19(b), a micrograph of the specimen after prestraining, the reflection was still largely characteristic radiation. However, this figure shows large areas where the (200) reflecting planes have rotated relative to other portions of the crystal so that no characteristic reflection was possible. Traces of kink bands, which were quite apparent after the creep test, appear to run diagonally up and to the right in figure 19(b). Therefore, the rotation observed in figure 19(b) can be attributed to the early onset of kinking. After the creep test the lattice was so distorted that one of the entrance slits had to be removed to get an exposure in a reasonable length of time. Hence, the height of the micrograph was increased slightly in addition to the increase in the horizontal scanning which resulted from an increased translation. In all cases these micrographs appear to be approximately twice as large as calculated from the translation and the magnification. The micrograph given as figure 19(c) shows considerable fine structure parallel to the slip lines in the reflections when viewed at 100X. Very little of the material in the irradiated area has been left intact to reflect the characteristic radiation because of the manner in which the crystal lattice has been broken up.

The manner in which the lattice breaks up during deformation has developed recently into a highly controversial issue. Wood and his English coworkers (refs. 35, 36, 37, 38, and 39) have supported a

fragmentation theory, according to which the lattice breaks up immediately into subgrains in order to allow deformation to take place along the subgrains or crystallite boundaries. The size of the subgrains formed in a polycrystalline material was found to be a function of the strain rate and the temperature. On the other hand, numerous other workers, including Cahn (refs. 40 and 41), Greenough and Smith (refs. 42 and 43), and Servi, Norton, and Grant (ref. 44), have concluded from similar experiments that the breakup of the crystalline lattice was a two-stage process in which plastic bending of the lattice planes was followed by polygonization. Polygonization is the process by which plastically bent and distorted regions can form a network of smaller regions which are relatively free of internal strains and which exhibit slight differences in orientation from one small region to the next. The plastic bending of the lattice produces an excess of dislocations of one sign. Then, at suitable temperatures, the stress-induced movement of the dislocations causes the dislocations to migrate along slip planes and to collect in localized regions to form an array of low-angle boundaries. Simultaneously, the segments of the lattice between the boundaries lose their curvature and elastic strain.

In a recent paper Gervais, Norton, and Grant (ref. 45) observed both types of subgrain formation. They found that the immediate fragmentation did take place in kinking but that most of the subgrain boundaries were formed by polyganization. They found little evidence of the flow along the subgrain boundaries predicted by Wood and his coworkers, but considerable rotation was observed to take place. In an investigation of the creep processes in coarse-grained aluminum (refs. 46, 47, and 48) McLean studied the formation of subgrains by using light microscopy and X-ray techniques. He observed no subboundaries during primary creep. Diffuse X-ray spots did not split into discrete spots until secondary creep had set in. From then on, the subgrain size decreased with increasing extension, being detected first near the grain boundaries and later in the interior of the grains. The disorientation of the subgrains also increased with extension. These disorientations were considerably larger than predicted by the observed subboundary movements. From this evidence McLean proposed a model in which the polygonization of the lattice into a substructure results in an observed extension. With this interpretation, polygonization, which contributes to the total deformation, can be termed a mechanism of deformation.

The X-ray work performed in this investigation, particularly the oblique Laue photographs, lends support to the views expressed by the second group of workers that the substructure is formed in a two-stage process. The oblique Laue photographs in figure 18 showed distortion of the lattice without any substructure formation after prestraining to a low extension at room temperature. The photographs taken after a creep test showed that a definite substructure had been formed during

creep. The reflection micrographs in figure 19 also indicated considerable rotation after the prestraining, but no fine substructure was detected until after the creep test. This evidence for a two-stage process in the formation of a substructure and the large rotations observed support McLean's conclusion that polygonization was definitely a mechanism of deformation, rather than a result of the deformation.

Operative Slip Systems at Elevated Temperatures

The operation of additional slip systems, especially at elevated temperatures, has been discussed by Chalmers and Martius (ref. 49) on the basis of the energy of dislocations and their associated slip planes. The slip direction is the most closely packed direction. This corresponds to the movement of those dislocations with the shortest possible Burgers vector, that is, the shortest unit slip distance in the slip direction necessary to bring the crystal lattice back into registry. For face-centered-cubic metals, such as aluminum, this direction is a [110] direction, and the unit slip distance is $a/(2)^{1/2}$, where a is the lattice parameter.

The energy of a dislocation must also depend on which slip plane is involved. Otherwise, any plane containing a [110] direction might operate at any temperature. Chalmers and Martius have taken this dependence to be a function of the shear strain, with the dislocations of lowest energy producing the lowest shear strain in a unit slip process. The shortest distances to the next parallel planes for the (111), (100), and (211) planes are $a/(3)^{1/2}$, $a/2$, and $a/2(6)^{1/2}$, respectively. The tangents of the angles of shear for the unit slip process are 1.225, 1.414, and 3.464, respectively, for these three planes with their associated [110] slip directions.

At room temperature only the (111) [110] slip system has been observed. However, as the temperature of deformation is increased, other systems have been observed to operate. In the cases reported, the systems reported have been ones which have a low value of shear strain for the unit slip process. Boas and Schmid (ref. 50) have observed slip in the (100) plane in a [110] direction in single crystals of aluminum at 450° C. More recently, Servi, Norton, and Grant (ref. 44) have shown that additional slip systems became operative during creep of high-purity coarse-grained aluminum at elevated temperatures. They found that the operative slip plane might be either a (100) plane or a (211) plane, in addition to the customary closed-packed (111) plane. In all cases the associated slip direction was one of the [110] close-packed directions located in the slip plane. However, the stress systems in polycrystalline materials are often quite complex.

With single-crystal specimens of known orientations it was possible to determine the effect of temperature on the operative slip system. Twenty-two crystals were deformed at temperatures from 300° to 1,100° F. All but one were deformed in constant-load creep tests, and 19 had one or more high-temperature slip systems containing a (100), (211), (311), or (110) plane, at least one of which was oriented more favorably than the most favorable system containing a (111) slip plane. Therefore, the resolved shear stress, or the value of $\cos \phi \cos \lambda$ which determines the fraction of the applied tensile stress which was resolved in the slip plane in the slip direction, was higher for a system containing one of the four high-temperature slip systems than for any system containing an octahedral slip plane. The pertinent data on these tests, presented in table 3, include the conditions of the test, the type of the primary operative slip plane and its orientation factor $\cos \phi \cos \lambda$, and the ratio of the resolved shear stress in the most favorably oriented high-temperature slip system to that in the most favorably oriented low-temperature slip system.

The results are presented graphically in figure 20. The ratio of the resolved shear stress on the favorably oriented high-temperature slip system, containing a (211), (100), (311), or (110) slip plane, to that on the most favorably oriented octahedral slip system has been plotted for each test temperature. To the left of the straight line, the slip plane was always an octahedral plane. To the right of the line, the slip plane was one of the four observed planes ((211), (100), (311), or (110)) in the system on which the resolved shear stress was the highest. The boundary line delineating octahedral slip from high temperature slip slopes down to the right from the lowest test temperature, 300° F, where a high-temperature slip system must be favored by approximately 40 percent to operate, to the point where a high-temperature slip system will operate at 900° F if it is equally favored or slightly more so. Because of the 12 slip systems containing a (111) plane and a [110] direction, one must be favored to some extent. Therefore, it is not possible to obtain crystals with high-temperature slip systems that are favored by more than 50 to 55 percent over the most favorably oriented octahedral slip system. The occurrence of slip on the (311) slip plane has been observed above 300° F; on the (100), above 500° F; on the (211), above 700° F; and on the (110) (one specimen), only at 1,000° F.

The onset of slip on these four high-temperature slip systems in aluminum demonstrates the increase in the ease of plastic deformation with the increase in the temperature at which the deformation takes place. As the temperature increases, the amplitude of vibration and the thermal energy of the atoms increase until the condition stated by Chalmers and Martius for the operative slip plane no longer holds. Then slip planes having slightly higher values of shear strain for the unit slip distance can operate also if they are oriented more favorably for slip than the most favorable system exhibiting the lowest value of shear strain for a unit slip distance. As the temperature is increased still further,

the amount by which the high-temperature slip system must be favored decreases in accord with the results shown in figure 20 for single crystals of high-purity aluminum.

Strain Markings by Light Microscopy

The details of kinking and slip-band formation have been observed by light microscopy. However, the structure of the slip bands must be studied with electron microscopy by replica techniques, and this work will be discussed in the next section.

The microscopic strain markings observed on five representative crystals are presented in figure 21. These micrographs were taken in a direction perpendicular to a plane containing the specimen axis and approximately parallel to the plane containing the slip direction. In all cases, the crystals were positioned so that the ends of the ellipses formed by the intersection of the slip bands with the specimen surface appear convex to the left and the kink bands appear convex to the right. The kink bands were observed on almost all crystals deformed in creep from 300° to 1,100° F, with no apparent dependence on the orientation of the specimen axis. The amount of kinking appeared to depend on the amount of deformation, on the temperature at which the deformation took place, and possibly on the strain rate. The kink bands were very sharp in the temperature range from 300° to 500° F. In figure 21(b), the observable bands are kink bands, which were much more prominent than the slip bands, which were not apparent in this micrograph. As the temperature was increased, the kink bands broadened out until they were barely noticeable in the creep specimen deformed at 1,100° F, as shown in figure 21(e). The kink bands were approximately perpendicular to the slip direction; that is, the slip direction was normal to the plane of the kink bands. These observations did not appear to depend on the primary operative slip plane, which was a (111) in figure 21(a), a (100) in figure 21(b), and a (211) in figures 21(c), 21(d), and 21(e).

Kinking presumably is the collection of an excess number of dislocations in a localized region. The physical appearance of the kink bands depends on the manner in which these dislocations are distributed, that is, whether they exist in a network or whether they have been collected in a boundary. Quite often the broad kink bands would either fade away or appear as a rumpled surface when viewed at higher magnifications. However, micrographs of the sharp kink bands were obtained at 100X from specimens deformed at 300° and 500° F. Three types of kink band that were observed in a Faxfilm replica of the surface are presented in figure 22. The most typical form of a kink band runs diagonally down and to the right in figure 22(a). Slip bands were observed to stop in the kink band, but no discrete difference in orientation was apparent.

In figure 22(b), the kink bands running diagonally up and to the right exhibited a sharp discontinuity in the surface in the kink band. When the specimen was viewed directly, instead of the replica, the difference in the reflections of light from the material on either side of the kink band provided evidence that there was a discrete difference in the orientation in this type of sharp kink band, which has been observed also by Gervais, Norton, and Grant (ref. 45). In the third type of kinking, duplex slip has been observed in the kink band in the upper-left-hand corner of figure 22(c).

Kinking does not take place in single crystals of zinc deformed in pure shear (ref. 34), but it does in zinc single-crystal tension specimens (ref. 51). Therefore, the bending moment which acts on a crystal deformed by creep in tension must be responsible for the occurrence of kinking. In addition, the slip planes rotate toward the tension axis as extension takes place, and the lattice on the opposite side of the crystal must deform to accommodate this rotation. Chen and Mathewson (ref. 52) have observed the formation kink bands in single crystals of aluminum that were very similar to the typical kink band shown in figure 22(a).

Gervais, Norton, and Grant (ref. 53) have investigated the role of the bending moment in kink-band formation. They concluded that slip on a second system could relieve the bending moment and prevent kinking. In an attempt to check this hypothesis, three specimens, S-3, S-13, and S-51, each with two favorably oriented slip systems, were deformed at 500° F in constant-load creep tests. The test conditions for these specimens have been included at the end of table 3. In crystals S-3 and S-51 duplex slip was not observed on a gross scale but only locally in the kink bands, as shown in figure 22(c). In crystal S-13, one slip system was operative on one end of the crystal and another on the other end. Kink bands were formed on each end of the specimen, and the only duplex slip on a gross scale was observed in the transition range between the two ends of the crystal. The deformation was too inhomogeneous to tell anything about kinking in this region. Because the specimens did not exhibit duplex slip on a gross scale, they did not prove or disprove whether duplex slip could eliminate kinking. However, they did indicate a tendency for duplex slip to take place on a fine, rather than a gross, scale at elevated temperatures. This tendency has also been observed in the electron-microscopy study of slip-band formation at elevated temperatures.

Low-magnification photographs of the slip bands are presented in figure 21. In general, the amount of shear on each slip band increased as the temperature was increased, that is, for a given strain. However, the most important observation to be made from these photographs is the difference between the slip bands formed at 1,100° F during a constant-load-rate test with a fairly rapid strain rate (see fig. 21(d)) and those

formed in a creep test with a relatively slower strain rate (see fig. 21(e)). The slow deformation was much more inhomogeneous. These gross slip bands observed on the creep specimen were actually made up of a number of slip bands which could be resolved easily at 100X. Other light micrographs of slip bands on specimens of the two purities are presented in figure 23. The slip bands on the high-purity crystal S-2 appeared quite broad and wavy at 100X after an extension of 9.3 percent at 500° F in 1.5 hours with 400-psi resolved shear stress. The slip bands on the low-purity crystal L-12 appeared relatively straight and much narrower at 250X after an extension of 14.4 percent in a constant-load-rate test at 500° F in 19 minutes. In addition, duplex slip on a gross scale was quite apparent in the lower purity specimen. These same observations were made in the electron micrographs at much higher magnifications.

Several speculative viewpoints have been expressed on slip-band formation, considerable experimental work has been done, and conclusions have been drawn from this work. However, no complete physical explanation has been put forth to explain why slip bands form as they do. The propagation of slip in high-purity aluminum single crystals at room temperature has been observed and photographed with a moving-picture camera by Chen and Pond (ref. 54). However, Brown (refs. 30, 55, 56, and 57) probably has done the most work on this problem of slip-band formation. In reference 55 Brown states that he found that the average number of individual lines in a slip band after 15 percent deformation increased with temperature, while the spacing decreased. The slip distance on an individual slip line decreased only slightly with temperature and was approximately 2,000 A at all temperatures from -180° to 500° C. In reference 30 Brown reports that the slip bands formed at room temperature were initially individual lines at low strains, and then the number of lines in a band increased as the strain was increased. He attempted to explain slip-band formation on the basis that slip took place in the regions of lowest hardness in the crystal and that a self-annealing process caused the hardness to be low in the region very close to the first and the subsequent slip lines in a slip band. This description must be considered weak, without any physical significance, until a physical picture of the self-annealing processes can be presented.

Recently, two suggestions for such a self-annealing process have been presented. Koehler (refs. 16 and 58) has suggested that the internal stresses resulting from thermal fluctuations can produce slip lamallae (individual lines) by allowing a screw dislocation to undergo cross slip and subsequent Frank-Read generation on a neighboring slip plane parallel to the initial locked lamella. This process would be dependent on the time involved in deformation, since longer times would allow more suitably large thermal fluctuations to activate the process more times in the same slip band. As evidence for this time dependence, Koehler

quoted Brown's results (ref. 30) that slip bands in aluminum strained rapidly at 450° C contained only 11 lamellae, whereas those formed in aluminum strained 1 percent per day at 450° C contained 50 lamellae.

The second suggestion for interpreting the structure of slip bands is based on a recovery model for the high-temperature creep process described by Sherby and Dorn (ref. 59). They have attributed the rate-controlling process to the recovery of barriers (to dislocation movement) by a self-diffusion process; that is, the barriers are reduced in strength, rather than being surmounted by thermally activated dislocations. At the temperatures at which diffusion is appreciable, it is also possible that a locked Frank-Read generator, such as the segment of an edge dislocation line in the slip plane, can climb perpendicular to the slip plane, by self-diffusion, to a neighboring plane, where it again can generate dislocations, resulting in another slip lamella in the slip band. This process would also be time dependent to the extent that specimens deformed in slow creep tests at high temperatures would be able to develop wide slip bands, whereas specimens deformed in relatively faster tensile tests would not have time to build up the large slip bands. These results are verified on a gross scale in figures 21(d) and 21(e). Details of the structure of the slip bands must be observed by electron microscopy. Regardless of the interpretation, the experimental results have shown that the structure of the slip bands at elevated temperature is dependent on the rate of straining. The relation is probably not simple but should be dependent on the recovery rate, which is a function of time, temperature, and possibly total strain.

Up to this point in the investigation, three mechanisms of creep, slip, kinking, and polygonization, have been observed. All three can be regarded as dislocation phenomena. They are probably all dependent on or interrelated to a recovery process involving either self-diffusion (ref. 59) or possibly the removal or redistribution of excess dislocations (ref. 60).

Electron-Microscope Observations

The results of the electron-microscope work are presented in the form of 16 micrographs in figures 24, 25, 26, and 27. Light micrographs have already been shown in figure 23 from two of the crystals from which electron micrographs were made.

Figures 24(a) and 24(b) show the elementary slip-line structures in specimens with relatively low strain. These figures are not representative of most of the surface area of the specimen, since most of the area shows no strain markings at all. Areas with slip-line markings such as those in the figures are seen in only about 1 percent of the surface

area scanned. In figure 24(a) the slip lines are nearly uniform, with the shear on each slip plane being about 400 A. This is in agreement with the data of Kuhlmann-Wilsdorf and Wilsdorf (refs. 61 and 62) for the magnitude of the elementary structure which they observed covering the entire surface between slip bands at high strains at room temperature. As can be seen in figure 24(a), even at low strain there is evidence of some duplex slip. It is not cross slip (i.e., slip on two planes in a common direction) because the slip directions are not the same in the two systems. This is consistent with the Kuhlmann-Wilsdorf hypothesis that aluminum contains many more possible Frank-Read sources (ref. 17) than can become active, because the dislocations from the different sources interfere strongly with each other's motion. Therefore, the yield stress for duplex slip may not be appreciably greater than that for single slip, depending on the crystal orientation. The spacing and over-all distribution of the slip lines is not in agreement with the results of Kuhlmann-Wilsdorf and Wilsdorf. This may be due partly to the fact that their observations were made on polycrystalline, rather than single-crystal, specimens.

There is no evidence of the 400 A elementary slip-line structure in any of the high-purity crystals deformed at elevated temperatures. The family of slip lines in figure 24(b) appears to have been generated from Frank-Read sources in the interior of the metal. In the widest portion of the slip lines the shear is probably between 1,500 A and 2,000 A. An accurate determination is difficult because there is no etch pit in the figure from which the orientation of the free surface can be calculated. The waviness of the slip lines at elevated temperatures is noticeable in figure 24(b). This can be attributed to several causes. The first cause is curvature of the lattice. However, this does not seem likely at such a low strain. The second cause is bending of the replica, which might create the illusion of curved lines. In view of the irregularity of the waviness, this does not appear to be likely. The most plausible explanation appears to be that these slip lines are not generated by a single Frank-Read source but by multiple sources on planes close together. It is entirely possible that a thinner replica, particularly a platinum replica, would disclose some fine structure in the wavy slip lines of figure 24(b), which was made from an aluminum-oxide replica. It seems probable that the dynamics of slip-line or slip-band (multiple lines) formation at elevated temperatures are more complex than the mechanisms based on Frank-Read sources and proposed by Fisher, Hart, and Pry (ref. 63) and other investigators.

The slip bands observed at low magnification after the deformation of high-purity aluminum at 500° F were also distinctly wavy, as shown in figure 23(a). Kuhlmann-Wilsdorf and Wilsdorf have suggested that the special form of the slip bands (i.e., whether they are wavy or straight) is determined very early in the deformation process. This

hypothesis, although interesting, is not very informative with regard to the dynamics of the process. This hypothesis is apparently borne out for the most part in aluminum specimens that were heavily deformed at room temperature. The slip lines and slip bands in heavily deformed aluminum (deformed by bending) are straight, as shown by two examples in figures 24(c) and 24(d). The slip in the easily resolved slip lines (e.g., the group of three spaced quite close together and running from the bottom center diagonally up and to the right in fig. 24(d)) exhibits a shear strain of 1,500 A to 2,000 A. However, there are evidently some finer slip lines which are not resolvable at a magnification of 10,000X in these particular replicas. It appears from figures 24(a), 24(c), and 24(d) that the shear along the slip plane in aluminum strained at room temperature varies from 400 A to several thousand angstroms. This is in disagreement with Brown's result (ref. 57) that the shear is uniformly about 2,000 A. It agrees with the observation of a considerable range in the shear on individual slip planes made by Kuhlmann-Wilsdorf and Wilsdorf (refs. 61 and 62).

Figures 25(a), 25(b), 26(c), and 26(d) show the surface structures in high-purity aluminum crystals deformed at elevated temperature. All of the specimens strained at 500° F show evidence of duplex slip on different planes in varying degrees. This indicates, as previously mentioned, an excess of Frank-Read sources. The slip band in figure 26(c) runs down and to the right. However, it should be mentioned that this structure was not typical of the surface. When the platinum replicas were examined under a vertical light microscope, slip bands were clearly visible. However, they almost always faded out when the objective lens current was turned on and the image enlarged and focused on the viewing screen. This is an indication that, when a high-purity aluminum crystal is deformed at elevated temperatures, the slip is too fine to be visible in the electron microscope. The step heights are probably less than 200 A. Only rarely was a band such as that one in figure 26(c) visible at high magnification. Originally, the structure in figure 26(c) was interpreted as a relatively fine slip on cubic planes (i.e., parallel to the side of the cubic etch pit in the lower right-hand corner) superimposed on a coarse slip on octahedral planes. However, in view of the fact that the slip bands are not generally visible at all in the electron microscope, this structure in figure 26(c) can be construed probably better as a group of narrow sub-bands with octahedral slip too fine to be resolved superimposed on resolvable cube slip. In any event, the slip in most of the bands must be fine slip because it was not generally visible in the electron microscope in replicas taken from high-purity crystals deformed in creep at elevated temperatures.

Bands in crystals deformed at 1,000° F sometimes appear straighter and narrower in the light microscope than bands in specimens strained at 500° F. The whole field in figure 26(d) would appear to be a single band in the light microscope at a magnification of 100X. The resolved

shear stress at 1,000° F is only about one-eighth that required to give an equivalent creep curve at 500° F in the high-purity aluminum. Evidently slip on parallel planes may be easier than multiple slip at this temperature. This depends, in part, on the crystal orientation. However, more work is needed in the examination of band structures at high magnification as a function of both temperature and strain rate, as there are insufficient data available at present to test theories of slip-band formation.

Figure 27 shows micrographs of band structures in a lower purity aluminum crystal strained rapidly at 500° F. The bands in figures 27(a), 27(b), and 27(c) run through etch pits. This band structure is quite complex. Apparently there are nearly equal slips on two sets of planes, giving a basket-weave structure. Which slip system appears more prominent depends on the orientation of the free surface. In some areas, such as in figure 27(d), the surface becomes so rumpled that the pattern no longer appears to be crystallographic in nature. This can be attributed to a displacement of the slip lines by the lines of the second system. If there are more than two systems operating, or if the slip alternates on first one system and then the other, the pattern can become nearly unrecognizable as a slip-system pattern, particularly for certain orientations of the free surface.

In an investigation of deformed polycrystalline aluminum with both Formvar and aluminum-oxide replicas, Garrod, Suitor, and Wood (ref. 64) observed that wavy slip bands were typical at elevated temperatures but offered no explanation. Trotter (ref. 65) made the same observation on coarse-grained high-purity aluminum deformed at 200° C in creep. However, he attributed the wavy nature of the slip lines to the occurrence of intimate cross slip.

In the lower purity aluminum, the displacement per slip plane is about 500 A, as compared with 2,000 A for the primary slip system in high-purity aluminum. The bands are narrower and straighter in the lower purity aluminum, as can be seen in the light micrographs in figures 23(a) and 23(b). Also, in the lower purity aluminum, there is duplex slip between the bands, as shown in figure 23(b) and in electron micrographs in figures 25(c) and 25(d). The indications are that there is still an excess of Frank-Read sources in the lower purity aluminum, so that most of the deformation takes place in the slip bands. However, the propagation of avalanches is hampered by the lattice defects around impurities, so that the strain per band is limited. If the strain is high enough, there is some cross slip between bands.

A subgrain structure in annealed polycrystalline aluminum was first noted by Robinson and Hunter (ref. 66) in electron micrographs from aluminum-oxide replicas of a chemically polished surface. This same

structure has been revealed in figures 26(a) and 26(b) in platinum replicas from an undeformed aluminum single crystal. Although this crystal actually was deformed, the surface was prepared before the deformation, and these micrographs from undeformed sections of the crystal are characteristic of a crystal as grown by the strain-anneal method. Figure 26(a) is probably the most striking of all the micrographs presented. All the smallest etch pits are located in subgrain or domain boundaries, whereas the somewhat larger ones are bisected by one of the boundaries. The facts that the boundaries are delineated by the chemical polish and that the etch pits originate in the boundaries indicate that these boundaries mark the sites of localized crystal imperfections of some sort. The most probable explanation is that they are the boundaries between small blocks slightly out of register. The continuous etching of the small boundaries might result from the elastically strained regions around the horizontal component of edge dislocations making up the straight boundaries. At higher magnification, such as in figure 26(b), the boundaries do not always appear continuous.

The dimensions of these blocks range from about 3/4 micron to 3 microns, or of the order of 1 micron. This range of size is particularly difficult to detect, since the particles are too small to yield individual X-ray reflections in anything but the best of microbeam techniques, and they are too large to cause X-ray line broadening. This mosaic structure has been predicted in the theory of imperfect crystals (ref. 67), and there is reason to believe that all metals are made up of such a characteristic structure. This small substructure undoubtedly plays a large part in determining the mechanical properties of metals. Wyon and Crussard (ref. 68) and Parker and coworkers (ref. 34) have carried out experiments indicating that the boundaries of a fine substructure, at least at low strains, will act as barriers to deformation. How this fine substructure detected in this investigation varies with annealing procedure remains to be seen.

The presence of this mosaic structure in a supposedly single crystal brings up the question of the distribution of dislocations in the annealed crystal. According to the dislocation model of a grain boundary, nearly all of the dislocations could be concentrated in the boundaries. Vogel, Pfann, and Corey (ref. 69) have observed etch pits in a low-angle boundary between two subgrains in germanium. They found that the etch pits developed at regular intervals along the boundary, the spacing being related to the observed difference in orientations of the two subgrains. Therefore, they concluded that the etch pits started at the intersection of the line of the edge dislocations in the boundary with the surface. More recently, Amelinckz (ref. 70) has found that etch pits developed on slightly deformed aluminum along the slip lines, along grain boundaries, and randomly. From the results of this investigation, the classification of "randomly," in all probability, refers to the etch pits formed at small subgrain or mosaic boundaries, as shown in figure 26(a).

At first sight, the hypothesis that all the dislocations are concentrated in the boundaries does not appear to be consistent with the presence of the elementary slip-line structure, as detected by Kuhlmann-Wilsdorf and Wilsdorf (refs. 61 and 62). They observed fine slip in aluminum with an average displacement of 300 A to 400 A per plane, with the lines spaced at approximately 400 A. However, when it is considered that the structure observed in figure 26(a) represents only the top layer and that there are many more layers below this one in offset positions, it is easy to see how the elementary lines can be so closely spaced, even if the dislocations and, hence, the Frank-Read sources are in these small boundaries, rather than inside the mosaic blocks. Again, regardless of the interpretation, any theory of slip-line formation must take into account the presence and the effect of this fine structure in the annealed crystals.

Some suggestions have been made in this section about future work. Basic to the theory of creep is the theory of slip-band formation. The electron microscope is probably the best single instrument for examination of slip bands. Improved surface-preparation and replica techniques enhance the value of this instrument. It probably would be advisable to use only high-purity aluminum in a fundamental study of slip-band formation. Crystals strained at various temperatures over a wide range of temperatures and with varying degrees of strain and strain rate would have to be examined. It probably would be profitable to examine the structure of a chemically polished surface after a low strain to see whether any relationship exists between the slip lines and the fine substructure, which indicates a definite ordering of at least one type of crystal imperfection.

SUMMARY OF RESULTS

The results of a study of plastic deformation of aluminum single crystals over a wide range of temperatures may be summarized as follows:

1. The effects of impurity content and temperature on the plastic properties of single crystals of aluminum have been observed in stress-strain curves determined by constant-load-rate tests at 82°, 500°, and 1,100° F on specimens of two purities.

2. The creep characteristics of high-purity aluminum single crystals have been determined for various stresses in the temperature range from 400° to 900° F under the condition of a constant resolved shear stress. No empirical relation has been obtained which could describe the creep data over the range of the variables investigated, presumably because of the differing kinetics of the mechanisms of deformation that have been observed.

3. The increased creep resistance provided by small amounts of prior strain was found to be determined by the details, such as temperature, strain rate, and amount of the prestrain.

4. The results of high-resolution X-ray techniques used to detect and to follow the internal strain throughout the various stages of a prestrain experiment showed the crystalline lattice to break up by a two-stage process involving plastic bending and subsequent polygonization.

5. At temperatures of about 300° F and above the operative slip plane could be a (311), a (110), a (100), or a (211) plane. The operative plane was the plane in the system on which the resolved shear stress was the highest, assuming that the slip direction was a [110] direction in all cases.

6. The details of kinking and slip-band formation in plastic deformation of single crystals of aluminum have been observed and recorded in light micrographs. Kink bands always form along planes to which the slip direction is normal. The formation of gross slip bands at elevated temperature appeared to be a function of the rate of strain.

7. A fine substructure, disclosed by means of a chemical polish, has been detected in annealed single crystals of high-purity aluminum. This structure has linear dimensions of the order of 1 micron.

8. Etch pits have been observed to originate in the boundaries between these small domains.

9. On crystals deformed at room temperature, shear displacements from 400 A to a few thousand angstroms have been observed on individual slip planes, or at least on fine slip bands which cannot be resolved at a magnification of 10,000X.

10. The amount of shear displacement per slip band has been observed to be considerably less in the lower purity specimens than in the high-purity specimens deformed to a comparable strain at the same elevated temperature.

11. Duplex slip has been observed within the band structure in specimens of both purities.

12. Duplex slip between the slip bands was much more apparent in the lower purity specimens in both the electron and the light micrographs.

13. The three mechanisms of plastic deformation by creep, slip, kinking, and polygonization, that have been detected can all be interpreted as dislocation phenomena.

Battelle Memorial Institute,
Columbus, Ohio, December 29, 1953.

REFERENCES

1. Schwope, A. D., and Jackson, L. R.: A Survey of Creep in Metals. NACA TN 2516, 1951.

2. Schwope, A. D., Shober, F. R., and Jackson, L. R.: Creep in Metals. NACA TN 2618, 1952.

3. Johnson, R. D., Shober, F. R., and Schwope, A. D.: The Creep of Single Crystals of Aluminum. NACA TN 2945, 1953.

4. Cottrell, A. H., and Aytekin, V.: The Flow of Zinc Under Constant Stress. The Jour. Inst. Metals, vol. 77, 1950, pp. 389-423.

5. Honeycombe, R. W. K.: A Simple Method of X-Ray Microscopy and Its Application to the Study of Deformed Metals. The Jour. Inst. Metals, vol. 80, pt. 1, Sept. 1951, pp. 39-44.

6. Keller, F.: Electron Microscopy of Light Metal Alloys. Symposium on Metallurgical Applications of the Electron Microscope, Inst. Metals (London), 1950, pp. 85-96.

7. Heidenreich, R. D., and Schockley, W.: Study of Slip in Aluminum Crystals by Electron Microscope and Electron Diffraction Methods. Conf. on Strength of Solids, Phys. Soc. (London), 1948, pp. 57-75.

8. Schwartz, C. M., Austin, A. E., and Weber, P. M.: A Positive-Replica Technique for Electron Microscopy. Jour. Appl. Phys., vol. 20, no. 2, Feb. 1949, pp. 202-205.

9. Austin, A. E., and Schwartz, C. M.: Modification of a Positive-Replica Technique for Electron Microscopy. Jour. Appl. Phys., vol. 22, no. 6, June 1951, pp. 847-848.

10. Hunter, M. S., and Robinson, D. L.: Techniques Used in Electron Microscopy of Aluminum Alloys. Symposium on Electron Metallography, A.S.T.M., June 1953. (To be published.)

11. Boas, W., and Schmid, E.: Über die Temperaturabhängigkeit der Kristallplastizität. Zs. Phys., Bd. 71, 1931, pp. 703-714.

12. Schmid, E., and Boas, W.: Plasticity of Crystals With Special Reference to Metals. F. A. Hughes and Co., Ltd. (London), 1950, pp. 58-59. (A translation.)

13. Cottrell, A. H.: Effect of Solute Atoms on the Behavior of Dislocations. Conf. on Strength of Solids, Phys. Soc. (London), 1948, pp. 30-38.

14. Taylor, G. I.: The Mechanism of Plastic Deformation of Crystals. Proc. Roy. Soc. (London), ser. A, vol. 145, no. 855, July 2, 1934, pp. 362-404.

15. Koehler, J. S.: On Dislocation Theory and the Physical Changes Produced by Plastic Deformation. Am. Jour. Phys., vol. 10, no. 6, Dec. 1942, pp. 275-285.

16. Koehler, J. S.: The Nature of Work-Hardening. Phys. Rev., vol. 86, no. 1, Apr. 1, 1952, pp. 52-59.

17. Frank, F. C., and Read, W. T., Jr.: Multiplication Processes for Slow-Moving Dislocations. Phys. Rev., second ser., vol. 79, no. 4, Aug. 15, 1950, pp. 722-723.

18. Cottrell, A. H.: The Yield Point in Single Crystal and Polycrystalline Metals. Symposium on the Plastic Deformation of Crystalline Solids, Carnegie Inst. Tech. and Office of Naval Res., NAVEXOS-P-834, May 19-20, 1950, pp. 60-76.

19. Hazlett, Thomas H., and Parker, Earl R.: Nature of the Creep Curve. Jour. Metals, vol. 5, no. 2, sec. 2 (Trans. Supp.), Feb. 1953, pp. 318-323. (See also Discussion by C. S. Roberts and N. J. Grant, Jour. Metals, vol. 5, no. 11, sec. 2 (Trans.), Nov. 1953, pp. 1577-1579.)

20. Bhattacharya, S., Congreve, W. K. A., and Thompson, F. C.: The Creep/Time Relationship Under Constant Tensile Stress. The Jour. Inst. Metals, vol. 81, pt. 2, Oct. 1952, pp. 83-92.

21. Andrade, E. N. daC.: On the Viscous Flow in Metals and Allied Phenomena. Proc. Roy. Soc. (London), ser. A, vol. 84, no. 567, June 9, 1910, pp. 1-12.

22. Roberts, C. S.: Creep Behavior of Extruded Electrolytic Magnesium. Jour. Metals, vol. 5, no. 9, Sept. 1953, pp. 1121-1126.

23. Wyatt, O. H.: Transient Creep in Pure Metals. Proc. Phys. Soc. (London), ser. B, vol. 66, no. 402, pt. 6, June 1, 1953, pp. 459-480.

24. Cottrell, A. H.: The Time Laws of Creep. Jour. Mech. and Phys. of Solids, vol. 1, no. 1, Oct. 1952, pp. 56-63.

25. Sherby, O. D., and Dorn, J. E.: Creep Correlations in Alpha Solid Solutions of Aluminum. Jour. Metals, vol. 4, no. 9, Sept. 1952, pp. 959-964.

26. Johnson, A. E., and Frost, N. E.: Rheology of Metals at Elevated Temperatures. Jour. Mech. and Phys. of Solids, vol. 1, no. 1, Oct. 1952, pp. 37-52.

27. Johnson, A. E., and Frost, N. E.: The Temperature Dependence of Transient and Secondary Creep of an Aluminum Alloy to British Standard 2L42 at Temperatures Between 20° and 250° C and at Constant Stress. The Jour. Inst. Metals, vol. 81, pt. 2, Oct. 1952, pp. 93-107.

28. Chang, H. C., and Grant, N. J.: Inhomogeneity in Creep Deformation of Coarse Grained High Purity Aluminum. Jour. Metals, vol. 5, no. 9, sec. 2 (Trans.), Sept. 1953, pp. 1175-1180.

29. Kennedy, A. J.: The Effect of Instantaneous Pre-Strain on the Character of Creep in Lead Polycrystals. Proc. Phys. Soc. (London), ser. B, vol. 62, no. 356, pt. 8, Aug. 1, 1949, pp. 501-508.

30. Brown, A. F.: Slip Bands and Hardening Processes in Aluminum. The Jour. Inst. Metals, vol. 80, pt. 3, Nov. 1951, pp. 115-125.

31. Rosi, F. D., and Mathewson, C. H.: A Study of the Plastic Behavior of High-Purity Aluminum Single Crystals at Various Temperatures. Jour. Metals, vol. 188, no. 9, Sept. 1950, pp. 1159-1167.

32. Ellis, W. C., and Greiner, E. S.: The Effect of Prior Strain at Low Temperatures on the Properties of Some Close-Packed Metals at Room Temperature. Jour. Metals, vol. 4, no. 6, June 1952, pp. 648-650.

33. Mott, N. F.: A Theory of Work-Hardening of Metals, II. Flow Without Slip-Lines, Recovery, and Creep. Phil. Mag., ser. 7, vol. 44, no. 354, July 1953, pp. 742-765.

34. Li, Choh Hsien, Washburn, J., and Parker, Earl R.: Variation of Plastic Properties With Annealing Procedure in Zinc Single Crystals. Jour. Metals, vol. 5, no. 9, sec. 2 (Trans.), Sept. 1953, pp. 1223-1225.

35. Wood, W. A.: The Lower Limiting Crystallite Structure Size and Internal Strains in Some Cold-Worked Metals. Proc. Roy. Soc. (London), ser. A, vol. 172, no. 949, Aug. 3, 1949, pp. 231-241.

36. Wilms, G. R., and Wood, W. A.: Mechanism of Creep in Metals. The Jour. Inst. Metals, vol. 75, pt. 8, Apr. 1949, pp. 693-706.

37. Wood, W. A., and Rachinger, W. A.: The Mechanism of Deformation in Metals, With Special Reference to Creep. The Jour. Inst. Metals, vol. 76, pt. 3, Nov. 1949, pp. 237-253.

38. Wood, W. A., and Scrutton, R. F.: Mechanism of Primary Creep in Metals. The Jour. Inst. Metals, vol. 77, pt. 5, Jan. 1950, pp. 423-434.

39. Wood, W. A., Wilms, G. R., and Rachinger, W. A.: Three Basic Stages in the Mechanism of Deformation of Metals at Different Temperatures and Strain Rates. The Jour. Inst. Metals, vol. 79, pt. 3, May 1951, pp. 159-172.

40. Cahn, R. W.: Recrystallization of Single Crystals After Plastic Bending. The Jour. Inst. Metals, vol. 76, pt. 2, Oct. 1949, pp. 121-143.

41. Cahn, R. W.: Slip and Polygonization in Aluminum. The Jour. Inst. Metals, vol. 79, pt. 3, May 1951, pp. 129-158.

42. Greenough, G. B., and Smith, E. M.: The Mechanism of Creep as Revealed by X-Ray Methods. The Jour. Inst. Metals, vol. 77, pt. 5, Jan. 1950, pp. 435-445.

43. Greenough, G. B., Bateman, C. M., and Smith, E. M.: X-Ray Diffraction Studies in Relation to Creep. The Jour. Inst. Metals, vol. 80, pt. 10, June 1952, pp. 545-550.

44. Servi, I. S., Norton, J. T., and Grant, N. J.: Some Observations of Subgrain Formation During Creep in High-Purity Aluminum. Jour. Metals, vol. 4, no. 9, Sept. 1952, pp. 965-971.

45. Gervais, Andre M., Norton, John T., and Grant, Nicholas J.: Subgrain Formation in High-Purity Aluminum During Creep at High Temperatures. Jour. Metals, vol. 5, no. 9, sec. 2 (Trans.), Sept. 1953, pp. 1166-1174.

46. McLean, D.: Creep Processes in Coarse-Grained Aluminum. The Jour. Inst. Metals, vol. 80, pt. 9, May 1952, pp. 507-519.

47. McLean, D.: Crystal Fragmentation in Aluminum During Creep. The Jour. Inst. Metals, vol. 81, pt. 6, Feb. 1953, pp. 287-292.

48. McLean, D.: Grain-Boundary Slip During Creep of Aluminum. The Jour. Inst. Metals, vol. 81, pt. 6, Feb. 1953, pp. 293-300.

49. Chalmers, B., and Martius, U. M.: Slip Planes and the Energy of Dislocations. Proc. Roy. Soc. (London), ser. A, vol. 213, no. 1113, June 24, 1952, pp. 175-185.

50. Boas, W., and Schmid, E.: The Dependence of Crystal Plasticity on Temperature. III - Aluminum. Zs. Phys., vol. 71, no. 11-12, 1931, pp. 703-714.

51. Washburn, J., and Parker, E. R.: Kinking in Zinc Single-Crystal Tension Specimens. Jour. Metals, vol. 4, no. 10, Oct. 1952, pp. 1076-1078.

52. Chen, N. K., and Mathewson, C. H.: Structural Studies of Plastic Deformation in Aluminum Single Crystals. Jour. Metals, vol. 3, no. 8, Aug. 1951, pp. 653-660.

53. Gervais, A. M., Norton, J. T., and Grant, N. J.: Kink Band Formation in High-Purity Aluminum During Creep at High Temperature. Jour. Metals, vol. 5, no. 11, sec. 2 (Trans.), Nov. 1953, pp. 1487-1492.

54. Chen, N. K., and Pond, R. B.: Dynamic Formation of Slip Bands in Aluminum. Jour. Metals, vol. 4, no. 10, Oct. 1952, pp. 1085-1092.

55. Brown, A. F.: Fine Structure of Slip Zones in Aluminum. Nature, vol. 163, no. 4155, June 18, 1949, pp. 961-962.

56. Brown, A. F., and Honeycombe, R. W. K.: Micro-Slip in Metal Crystals. Phil. Mag., vol. 42, no. 333, Oct. 1951, pp. 1146-1149.

57. Brown, A. F.: Surface Effects in Plastic Deformation of Metals. Advances in Phys., vol. 1, no. 4, Oct. 1952, pp. 427-479.

58. Koehler, J. S.: Theory of Initial Stress-Strain Curves in Face-Centered Metals. Acta Metallurgica, vol. 1, no. 3, May 1953, p. 377.

59. Sherby, O. D., and Dorn, J. E.: A Recovery Model for the High Temperature Creep Process. Tech. Rep. 30, Ser. No. 22, Contract N7-onr-295, Task Order II, Project NR-031-048, Office of Naval Res. and Inst. Eng. Res., Univ. of Calif., Aug. 15, 1953.

60. Drouard, R., Washburn, J., and Parker, Earl R.: Recovery in Single Crystals of Zinc. Jour. Metals, vol. 5, no. 9, sec. 2 (Trans.), Sept. 1953, pp. 1226-1229.

61. Kuhlmann-Wilsdorf, D., Van der Merwe, J. H., and Wilsdorf, H.: Elementary Structure and Slip-Band Formation in Aluminum. Phil. Mag., vol. 43, no. 341, June 1952, pp. 632-643.

62. Kuhlmann-Wilsdorf, Doris, and Wilsdorf, Heinz: The Surface Structures of Deformed Aluminum, Copper, Silver, and Alpha-Brass, and Their Theoretical Interpretation. Acta Metallurgica, vol. 1, no. 4, July 1953, pp. 394-413.

63. Fisher, J. C., Hart, E. W., and Pry, R. H.: Theory of Slip-Band Formation. Phys. Rev., second ser., vol. 87, no. 6, Sept. 15, 1952, pp. 958-961.

64. Garrod, R. I., Suiter, J. W., and Wood, W. A.: An Electron-Microscope Study of the Effect of Temperature and Strain-Rate on the Mechanism of Deformation of Aluminum. Phil. Mag., vol. 43, no. 341, June 1952, pp. 677-685.

65. Trotter, J.: Electron-Microscope Studies of Slip in Aluminum During Creep. The Jour. Inst. Metals, vol. 80, pt. 9, May 1952, pp. 521-523.

66. Hunter, M. S., and Robinson, D. L.: Revealing the Subgrain Structure of Aluminum. Jour. Metals, vol. 5, no. 5, sec. 2 (Trans. Supp.), May 1953, pp. 717-722.

67. Zachariasen, W. H.: Theory of X-Ray Diffraction in Crystals. John Wiley & Sons, Inc., 1945, p. 161.

68. Wyon, G., and Crussard, C.: Alterations of the Structure of Aluminum During Creep. Rev. métallurgie, vol. 48, pt. 2, Feb. 1951, pp. 121-130. (Translated by R. F. Flint, Fulmer Res. Inst., Ltd., Trans. No. 17.)

69. Vogel, F. L., Pfann, W. G., Corey, H. E., and Thomas, E. E.: Observations of Dislocations in Lineage Boundaries in Germanium. Phys. Rev., second ser., vol. 90, no. 3, May 1, 1953, pp. 489-490.

70. Amelinckz, S.: Slip Lines and Etch Pits. Phil. Mag., vol. 44, ser. 7, no. 356, Sept. 1953, pp. 1048-1049.

TABLE 1.- SUMMARY OF RESULTS OF CRYSTAL GROWTH

Crystal size, in.	Number of crystals at prestrain, percent, of -					Total
	2	$1\frac{1}{2}$	$1\frac{1}{4}$	1	2/3	
	First growth - 54 specimens[a]					
1	[b]4	5	--	1	--	10
1	[b]4	11	--	5	--	20
2	[b]2	3	--	0	--	5
3	[b]2	12	--	5	--	19
Total	12	31		11		54
	Second growth - 54 specimens[a]					
1	1	3	2	4	1	11
1	0	3	1	2	2	8
2	0	1	2	4	6	13
3	0	2	5	14	1	22
Total	1	9	10	24	10	54

[a]All from aluminum of 99.99+-percent purity unless otherwise indicated.

[b]From aluminum of 99.95-percent purity.

TABLE 2.- CRYSTALLOGRAPHIC DATA FOR ALUMINUM SINGLE CRYSTALS

Crystal	Slip plane	α	β	χ	ϕ	λ	Cos ϕ cos λ
Crystals for constant-load-rate tests							
L-3	(111)	[a]26.0	15.5	59.4	53.5	[a]37.0	0.474
	(111)				[a]25.7	65.5	.373
	(111)				[a]66.0	23.5	.372
L-5	(111)	[a]31.5	11.3	55.8	49.2	[a]43.7	.470
	(111)				26.7	63.5	.398
	(111)				49.2	[a]59.5	.330
L-12	(111)	[a]32.0	[a]8.0	56.5	[a]45.0	46.7	.485
	(111)				30.0	[a]60.5	.426
	(111)				[a]45.0	61.5	.337
S-23	(111)	13.0	[a]12.0	71.5	57.0	[a]34.0	.450
	(111)				[a]57.5	34.0	.445
	(111)				36.0	59.5	.410
S-56	(111)	[a]57.5	7.8	31.3	[a]45.3	46.3	.486
	(111)				[a]30.0	60.1	.431
	(111)				[a]45.3	[a]62.0	.330
S-64	(111)	7.0	[a]48.0	41.0	42.5	[a]53.0	.445
	(111)				42.5	[a]57.0	.402
	(211)				37.5	[a]53.0	.477
Crystals for constant-stress creep tests							
S-6	(111)	5.8	[a]71.7	[a]17.0	49.8	[a]42.0	0.480
	(111)				[a]39.7	53.0	.462
	(111)				[a]64.0	28.3	.371
S-7	(111)	[a]12.0	63.0	22.0	[a]51.5	38.0	.491
	(111)				30.0	[a]61.0	.420
	(111)				65.5	[a]24.0	.379
S-10	(111)	[a]24.2	7.6	64.2	47.5	[a]43.0	.493
	(111)				[a]33.3	57.5	.448
	(111)				78.2	78.6	.397
S-14	(111)	[a]28.5	[a]56.7	15.5	52.5	[a]39.0	.472
	(111)				[a]24.0	66.5	.363
	(111)				[a]69.0	21.5	.332
S-16	(111)	[a]22.0	[a]60.5	18.0	57.5	[a]33.0	.450
	(111)				[a]61.5	29.0	.417
	(111)				[a]26.0	67.0	.350
S-25	(111)	[a]37.0	[a]49.5	13.0	48.5	[a]45.0	.468
	(111)				48.5	[a]54.0	.389
	(111)				[a]23.0	68.0	.344
S-34	(111)	[a]12.0	[a]12.0	73.0	[a]56.8	34.5	.452
	(111)				[a]58.2	33.0	.440
	(111)				36.5	[a]59.0	.413
S-35	(111)	[a]55.0	31.0	12.5	49.0	[a]43.5	.475
	(111)				[a]26.0	64.5	.386
	(111)				49.0	[a]60.0	.328

[a]Measured from left end of specimen; all others measured from right.

TABLE 2.- CRYSTALLOGRAPHIC DATA FOR ALUMINUM SINGLE CRYSTALS - Continued

Crystal	Slip plane	α	β	χ	ϕ	λ	Cos ϕ cos λ
Crystals for constant-stress creep tests - Concluded							
S-36	(111) (111) (111)	[a]58.8	[a]24.8	17.0	55.5 [a]65.0 [a]25.0	[a]35.7 25.5 66.7	0.460 .381 .358
S-50	(111) (111) (111)	[a]38.0	[a]48.7	12.6	48.5 48.5 [a]23.1	[a]46.5 [a]53.9 67.9	.456 .391 .346
S-57	(111) (111) (111)	[a]28.4	11.2	58.7	48.9 [a]28.1 [a]70.5	[a]42.0 62.0 19.2	.488 .414 .315
S-66	(111) (111) (111)	[a]12.0	[a]57.5	30.0	[a]49.5 26.5 [a]49.5	42.0 [a]63.5 [a]60.0	.482 .399 .325
S-75	(111) (111) (111)	[a]15.2	[a]26.7	58.6	[a]53.1 25.6 67.1	[a]38.1 [a]65.0 23.2	.472 .382 .357
Crystals for electron-microscope work							
L-6	(111) (111) (111)	[a]63.0	7.8	25.8	46.7 [a]32.8 70.2	43.7 57.7 [a]20.8	0.495 .449 .315
L-11	(111) (111) (111)	[a]20.0	18.5	62.0	58.5 [a]60.0 27.5	[a]31.0 30.5 66.5	.447 .430 .353
S-2	(111) (111) (111)	[a]17.5	[a]50.0	34.0	[a]53.5 [a]53.5 19.0	41.0 [a]52.5 [a]71.5	.447 .361 .299
S-9	(111) (111) (111)	[a]63.5	22.5	13.0	[a]52.0 [a]30.5 65.0	38.0 62.0 [a]26.0	.484 .403 .378
S-37	(111) (111) (111)	[a]52.3	24.0	26.8	61.3 64.0 61.3	32.3 28.3 [a]53.0	.404 .385 .288
S-38	(111) (111) (111)	.2	[a]36.2	52.5	36.2 [a]36.2 36.2	[a]55.5 56.0 [a]65.0	.456 .450 .340
P-175	(111) (111) (111)	[a]41.5	[a]8.1	46.9	[a]43.9 [a]43.9 28.0	52.0 55.6 [a]65.2	.444 .407 .370
P-181	(111) (111) (111)	[a]15.9	27.0	57.5	[a]53.6 24.0 67.7	37.8 [a]66.2 [a]22.8	.468 .369 .349

[a]Measured from left end of specimen; all others measured from right.

TABLE 2.- CRYSTALLOGRAPHIC DATA FOR ALUMINUM SINGLE CRYSTALS - Continued

Crystal	Slip plane	α	β	χ	ϕ	λ	Cos ϕ cos λ
Crystals for prestrain experiments							
S-5	(111)	[a]9.5	[a]52.5	35.7	[a]45.5	47.5	0.473
	(111)				27.7	[a]63.5	.394
	(111)				[a]45.5	58.2	.368
S-8	(111)	[a]34.7	[a]11.0	53.0	[a]47.3	45.3	.475
	(111)				26.0	[a]64.7	.383
	(111)				[a]47.3	57.3	.364
S-12	(111)	[a]47.5	[a]38.2	15.5	51.5	[a]44.5	.443
	(111)				51.5	[a]51.2	.389
	(111)				[a]20.5	70.2	.315
S-17	(111)	[a]10.7	39.5	48.2	[a]46.5	49.0	.451
	(111)				[a]46.5	54.3	.401
	(111)				24.7	[a]66.5	.361
S-43	(111)	[a]23.3	45.3	35.2	[a]59.0	38.5	.403
	(111)				[a]59.0	46.4	.355
	(111)				72.5	[a]24.0	.275
S-44	(111)	[a]44.5	[a]36.1	23.3	58.8	[a]39.0	.402
	(111)				58.8	[a]46.0	.360
	(111)				[a]73.1	23.9	.266
S-58	(111)	[a]29.6	[a]21.3	52.0	[a]58.2	35.5	.429
	(111)				[a]68.0	[a]24.8	.341
	(111)				18.1	[a]72.6	.284
S-62	(111)	[a]46.2	[a]10.3	41.8	[a]45.7	50.6	.443
	(111)				[a]45.7	53.5	.415
	(111)				25.4	67.3	.349
S-67	(111)	[a]59.6	[a]20.0	21.7	[a]58.8	31.7	.441
	(111)				61.4	29.0	.419
	(111)				24.8	[a]68.1	.339
S-70	(111)	[a]27.0	16.0	58.0	54.0	[a]37.5	.466
	(111)				24.5	[a]66.5	.363
	(111)				[a]67.0	23.0	.360
S-73	(111)	[a]9.7	[a]37.0	50.7	[a]45.7	[a]47.9	.468
	(111)				26.7	[a]64.4	.386
	(111)				[a]45.7	56.9	.381
S-76	(111)	[a]54.3	30.3	17.0	54.0	38.8	.458
	(111)				[a]21.8	68.6	.339
	(111)				54.0	[a]55.8	.330
S-78	(111)	[a]9.7	[a]25.7	62.0	[a]48.5	42.0	.493
	(111)				31.2	[a]59.7	.432
	(111)				69.2	[a]21.3	.331
S-86	(111)	[a]30.1	[a]15.0	55.6	52.3	[a]39.9	.469
	(111)				23.9	[a]66.5	.365
	(111)				52.3	57.5	.329

[a]Measured from left end of specimen; all others measured from right.

TABLE 2.- CRYSTALLOGRAPHIC DATA FOR ALUMINUM SINGLE CRYSTALS - Continued

Crystal	Slip plane	α	β	χ	ϕ	λ	Cos ϕ cos λ
Crystals for prestrain experiments - Concluded							
S-94	(111) (111) (111)	[a]6.5	[a]37.0	52.0	[a]42.3 29.7 [a]42.3	50.2 [a]61.7 59.5	0.472 .411 .375
Crystal for X-ray work							
S-63		[a]51.4	[a]36.8	8.9	44.6 [a]27.5 44.6	[a]48.4 63.5 [a]58.0	0.473 .396 .377
Crystals for constant-load creep tests							
P-149	(100) (211) (100) (111) (111)	[a]22.3	36.7	44.6	[a]45.4 [a]51.3 [a]53.3 [a]58.0 [a]58.0	46.1 40.0 40.0 40.0 46.1	0.486 .479 .458 .406 .367
P-159	(100) (311) (111)	[a]25.3	44.3	34.9	[a]45.7 [a]53.0 [a]60.8	45.1 37.5 37.5	.493 .477 .387
P-169	(100) (111) (111)	[a]22.2	53.1	27.4	[a]36.9 [a]59.4 65.5	53.8 34.0 [a]26.8	.473 .422 .371
S-1	(100) (111) (111)	[a]27.7	[a]47.5	29.0	42.5 [a]64.3 65.5	[a]47.7 31.5 [a]30.0	.495 .368 .358
S-3	(111) (111) (111)	.7	[a]21.0	68.7	42.5 41.0 41.0	[a]48.0 49.7 66.0	.493 .488 .306
S-13	(111) (111) (111)	[a].5	28.7	[a]61.0	[a]39.0 37.7 [a]39.0	51.3 52.5 69.7	.485 .480 .269
S-18	(211) (100) (100) (111) (111)	[a]13.34	[a]44.00	42.7	[a]42.0 46.0 [a]47.3 [a]49.3 [a]49.3	49.0 [a]50.0 49.0 49.0 [a]50.0	.487 .447 .443 .428 .419
S-20	(100) (111) (111)	[a]26.0	[a]54.0	23.0	36.0 60.5 [a]64.0	[a]54.0 [a]32.0 28.0	.475 .417 .386
S-21	(100) (100) (311) (211) (111) (111)	[a]30.7	36.3	38.0	[a]52.0 [a]53.7 [a]54.5 [a]58.5 [a]66.5 [a]66.5	38.5 37.0 38.5 37.0 37.0 38.5	.481 .472 .454 .417 .318 .311

[a]Measured from left end of specimen; all others measured from right.

TABLE 2.- CRYSTALLOGRAPHIC DATA FOR ALUMINUM SINGLE CRYSTALS - Concluded

Crystal	Slip plane	α	β	χ	ϕ	λ	Cos ϕ cos λ
Crystals for constant-load creep test - Concluded							
S-27	(211)	[a]27.5	[a]16.0	56.0	54.0	[a]36.5	0.472
	(111)				56.0	[a]36.5	.448
	(100)				[a]34.0	57.5	.445
	(111)				[a]68.0	22.5	.345
S-39	(211)	[a]38.5	[a]13.5	49.0	[a]44.5	46.0	.496
	(111)				[a]49.0	46.0	.456
	(100)				[a]41.0	53.0	.454
	(111)				[a]49.0	53.0	.394
S-42	(211)	[a]49.0	35.0	10.5	50.0	40.5	.489
	(100)				41.0	[a]51.2	.471
	(111)				54.3	40.5	.443
	(111)				54.3	[a]51.2	.364
S-45	(100)	[a]34.1	29.5	41.4	[a]48.6	42.0	.491
	(100)				55.9	[a]35.0	.459
	(211)				58.5	[a]35.0	.428
	(111)				65.0	[a]35.0	.346
	(111)				65.0	42.0	.314
S-46	(100)	[a]30.4	26.9	46.7	[a]43.3	[a]47.2	.494
	(211)				58.0	[a]33.2	.444
	(111)				62.8	[a]33.2	.383
	(111)				[a]67.2	28.9	.340
S-51	(111)	[a]70.5	19.2	.6	[a]42.3	48.6	.489
	(111)				43.1	[a]48.0	.488
	(111)				[a]42.3	64.3	.321
S-60	(100)	[a]29.0	[a]35.5	41.0	[a]49.0	41.0	.495
	(100)				54.5	[a]36.0	.470
	(211)				57.5	[a]36.0	.434
	(111)				65.0	[a]36.0	.342
	(111)				65.0	41.0	.319
S-71	(100)	[a]33.1	[a]40.7	30.7	49.3	[a]41.4	.489
	(100)				56.9	[a]34.1	.452
	(111)				66.3	[a]34.1	.333
	(111)				[a]69.1	30.7	.307
S-77	(100)	[a]23.5	39.0	41.0	[a]49.0	43.0	.480
	(100)				[a]51.0	41.5	.471
	(111)				[a]59.0	41.5	.386
	(111)				[a]59.0	43.0	.376
S-82	(100)	[a]36.1	38.2	30.9	[a]51.8	38.7	.482
	(100)				53.9	[a]36.5	.474
	(111)				66.4	[a]36.5	.322
	(111)				66.4	38.7	.312
S-84	(311)	[a]41.3	18.8	42.3	45.5	[a]45.7	.488
	(100)				[a]47.7	[a]45.9	.468
	(211)				47.3	[a]45.7	.473
	(111)				54.0	[a]45.7	.410
	(111)				54.0	[a]45.9	.409
S-87	(110)	[a]79.5	[a]3.7	9.7	[a]50.0	42.3	.475
	(111)				[a]51.0	42.3	.465

[a]Measured from left end of specimen; all others measured from right.

TABLE 3.- SUMMARY OF DATA ON OPERATIVE SLIP PLANE AT ELEVATED TEMPERATURES

Crystal	Temperature, °F	Test (a)	Strain, ϵ	Primary operative plane		
				Type	Cos ϕ cos λ	$\frac{\tau(\text{high-temperature system})}{\tau(111)}$
S-21	300	400-psi RSS for 10 min	0.005	(311)	0.454	1.43
S-20	500	300-psi RSS for 25.4 hr	.124	(111)	.417	1.139
S-82	500	450-psi RSS for 140 min	.078	(100)	.482	1.497
P-169	700	75-psi RSS for 67 hr	.025	(111)	.422	1.121
P-159	700	100-psi RSS for 18.5 hr	.098	(311)	.477	1.23
S-18	700	182-psi RSS for 46 min	.12	(211)	.487	1.14
S-71	700	147-psi RSS for 5.3 hr	.10	(100)	.489	1.468
S-60	800	109-psi RSS for 278 min	.165	(100)	.495	1.447
S-27	900	79-psi RSS for 168 min	.10	(211)	.472	1.054
S-46	900	75-psi RSS for 100 min	.11	(100)	.494	1.290
S-45	900	71.0-psi RSS for 100 min	.117	(100)	.491	1.418
S-87	1,000	50-psi RSS for 15 min	.10	(110)	.475	1.02
S-77	1,000	62.2-psi RSS for 18 min	.10	(100)	.480	1.244
S-1	1,000	67.3-psi RSS for 25 min	.216	(100)	.495	1.345
S-64	1,100	CLR in 6 min	.13	(211)	.477	1.072
S-39	1,100	27.2-psi RSS for 66 hr	.129	(211)	.496	1.088
S-42	1,100	27.6-psi RSS for 5.2 hr	.14	(211)	.489	1.104
S-84	1,100	28.8-psi RSS for 6 hr	.20	(311)	.488	1.19
P-149	1,100	29.9-psi RSS for 20 hr	.35	(100)	.486	1.197
S-3	500	400-psi RSS for 3.3 hr	.115	(111)	.493	
S-13	500	400-psi RSS for 45 min	.10	(111)	.485 .480	
S-51	500	600-psi RSS for 1 min	.15	(111)	.489	

[a]RSS, resolved shear stress; CLR, constant load rate.

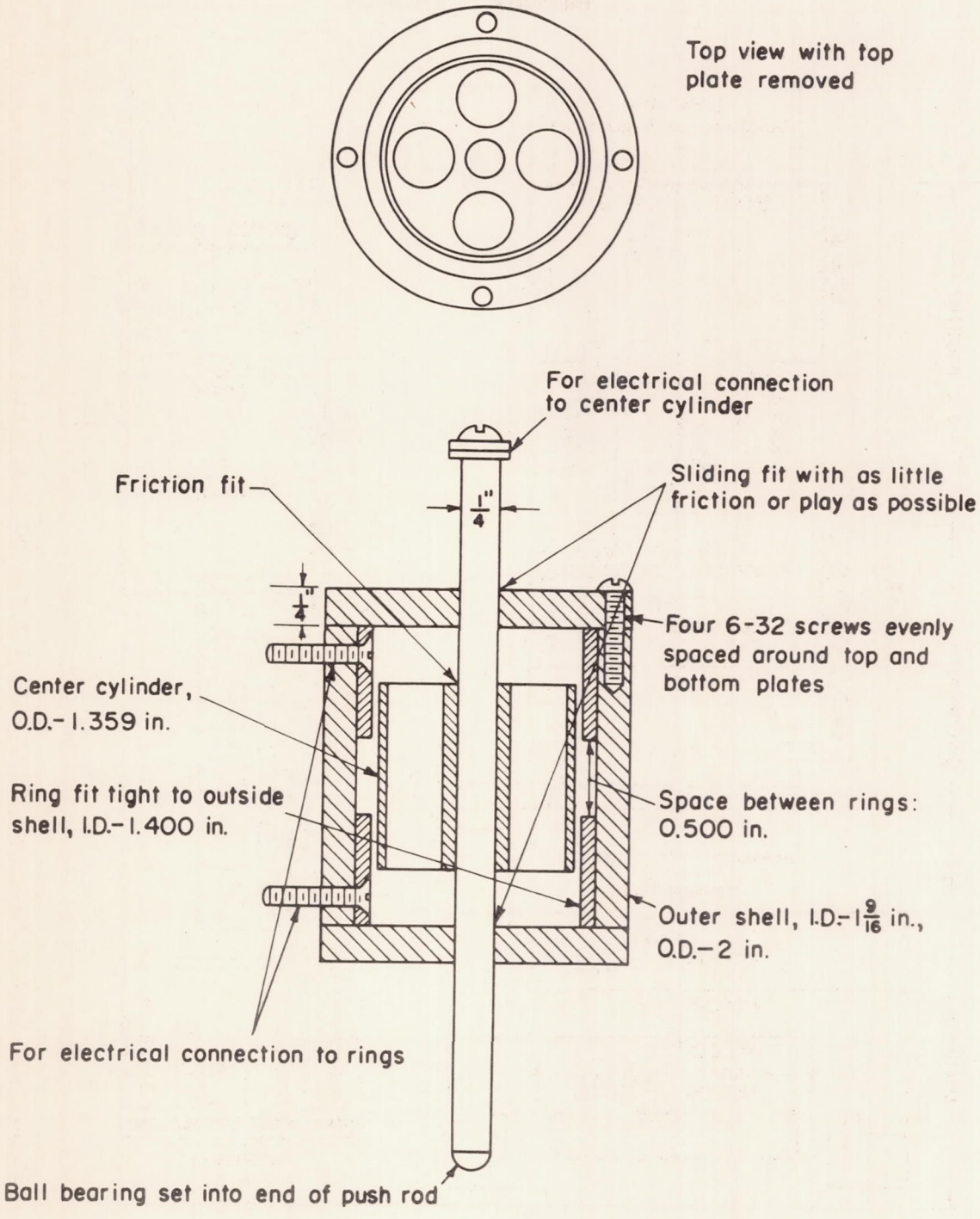


Figure 1.- Capacitance pickup with cylindrical plates. Materials: Cylindrical plates and push rod are commercial 2S aluminum; outside case is Lucite.

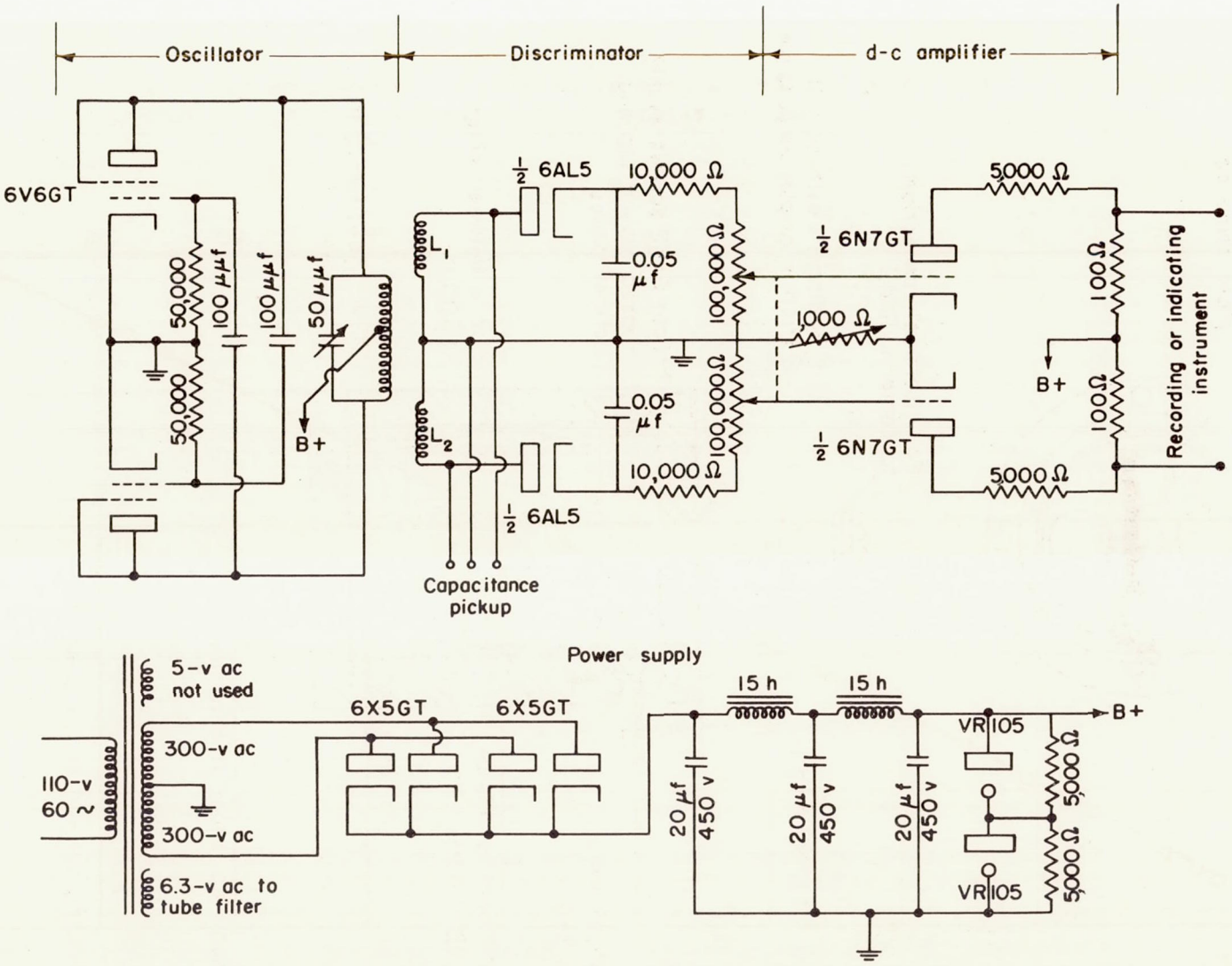


Figure 2.- Capacitance-measuring unit for cylindrical-plate pickup.

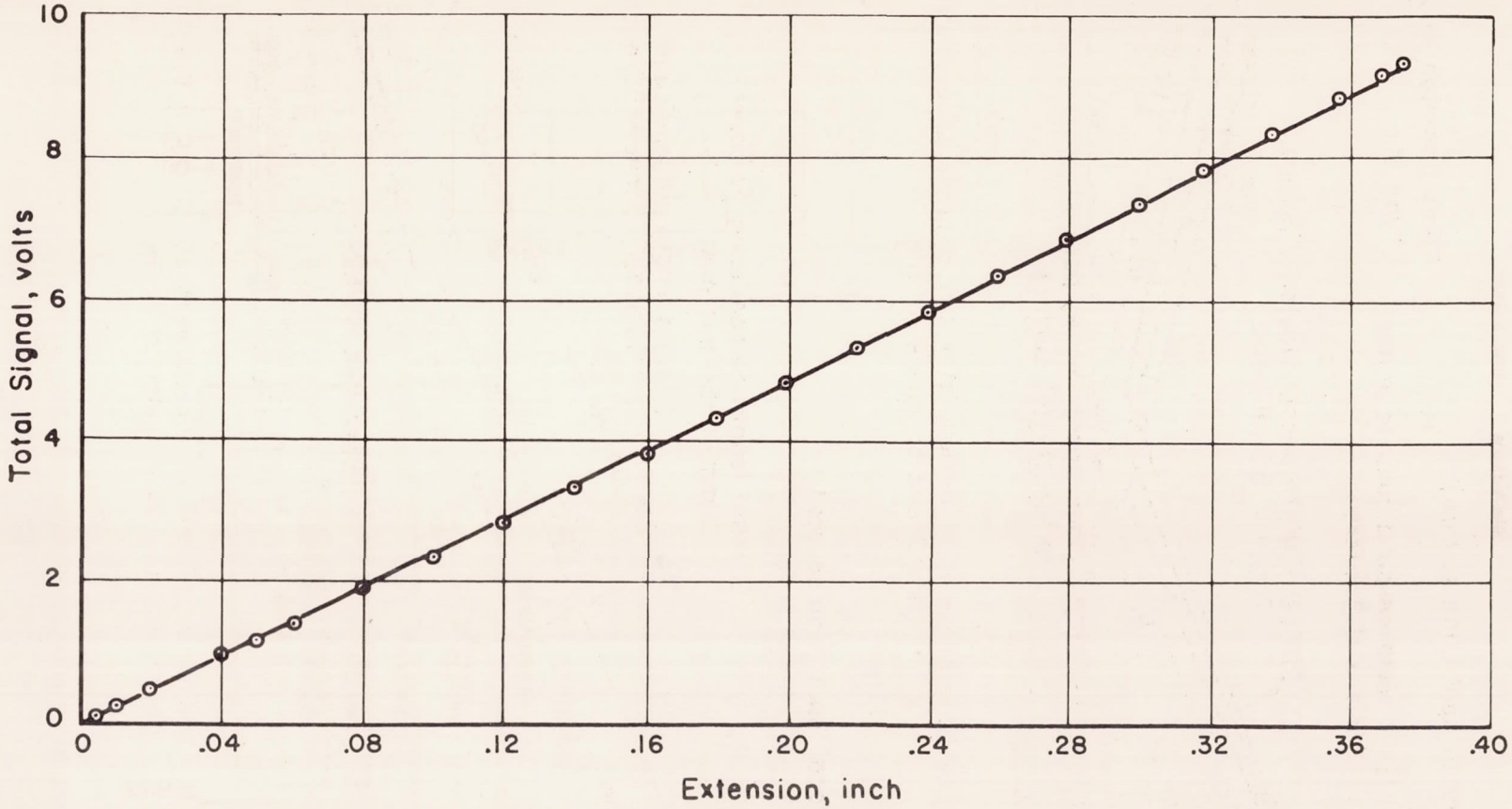


Figure 3.- Calibration plot for cylindrical-plate pickup. Sensitivity, 41 microinches per millivolt over a range of 0.30 inch.

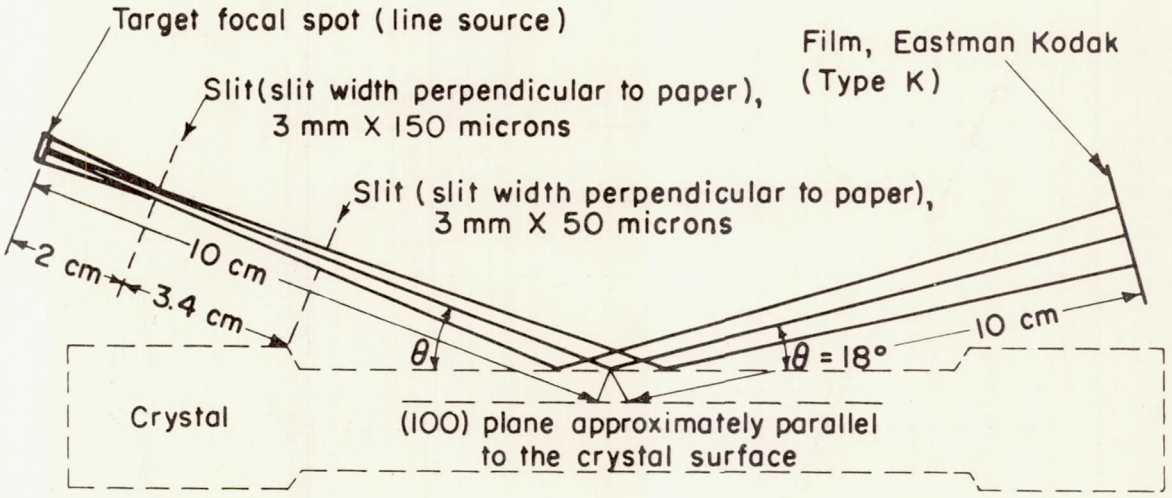


Figure 4.- Top view of experimental arrangement for oblique Laue photographs. (Not drawn to scale.)

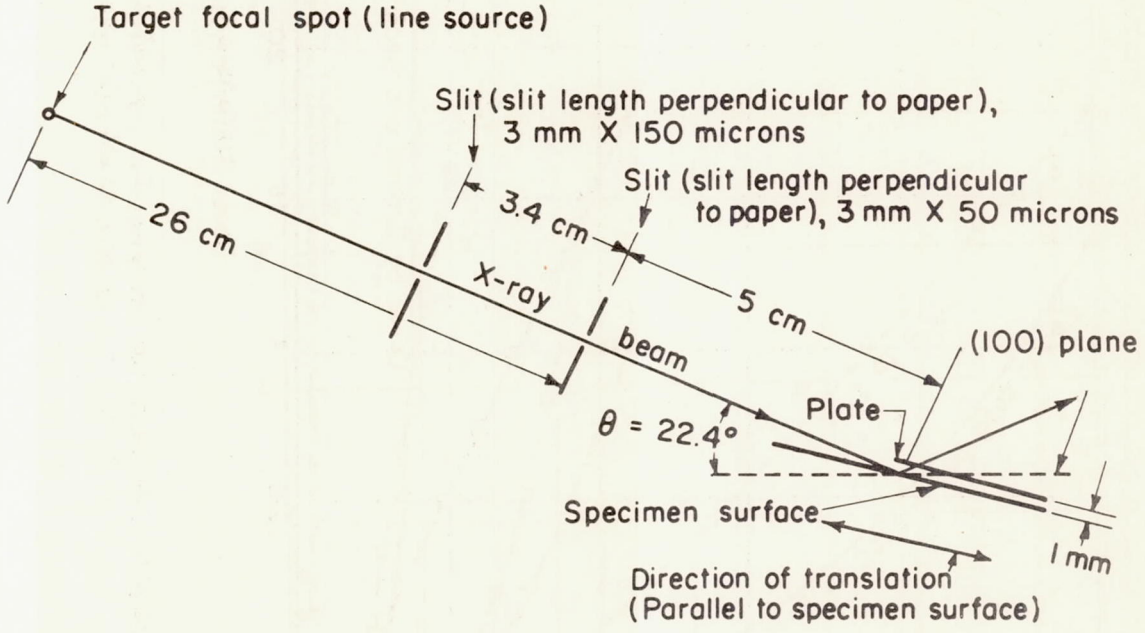


Figure 5.- Top view of experimental arrangement for X-ray reflection micrographs. (Not drawn to scale.)

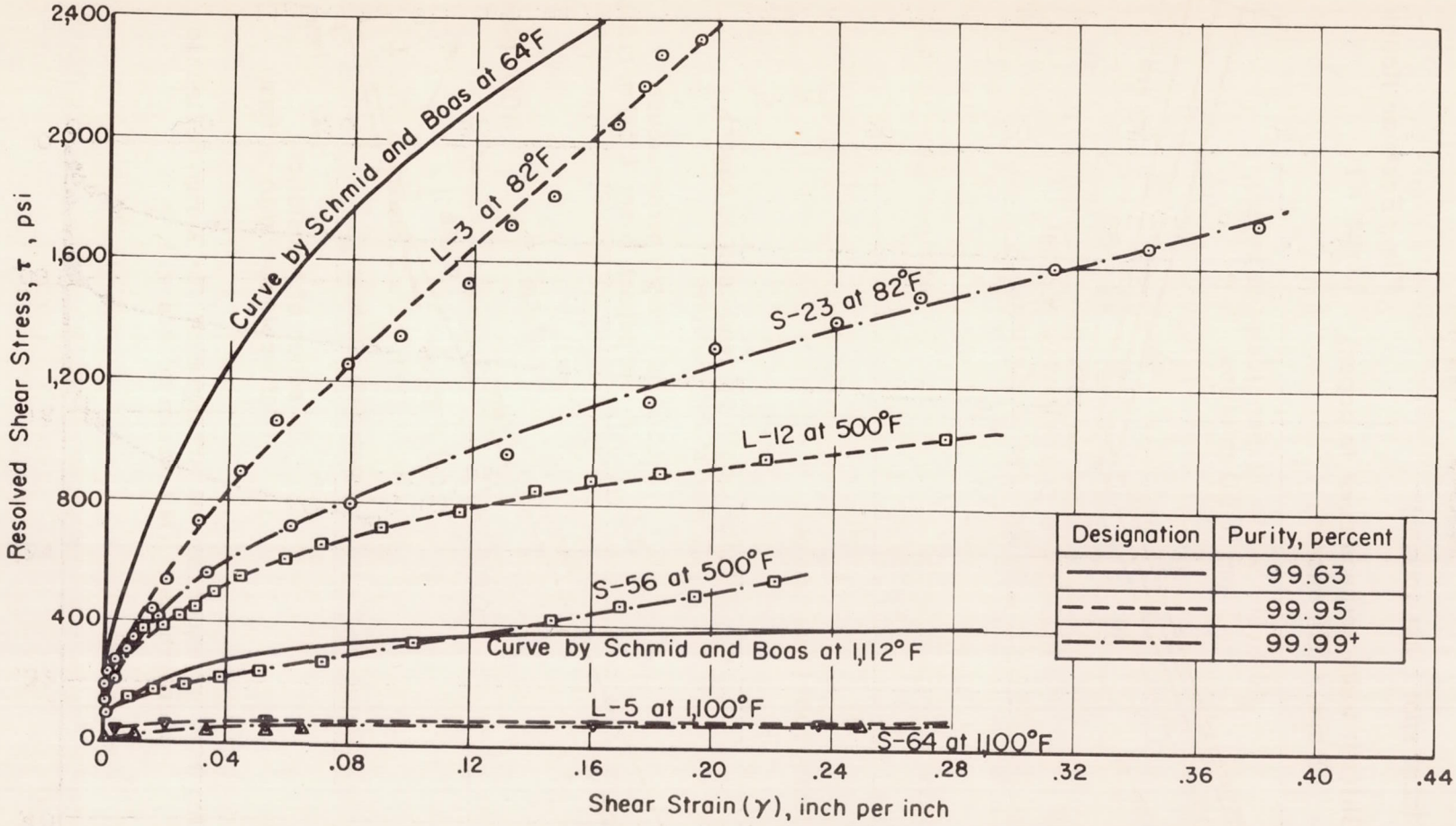


Figure 6.- Effects of temperature and purity on stress-strain curves of aluminum single crystals.

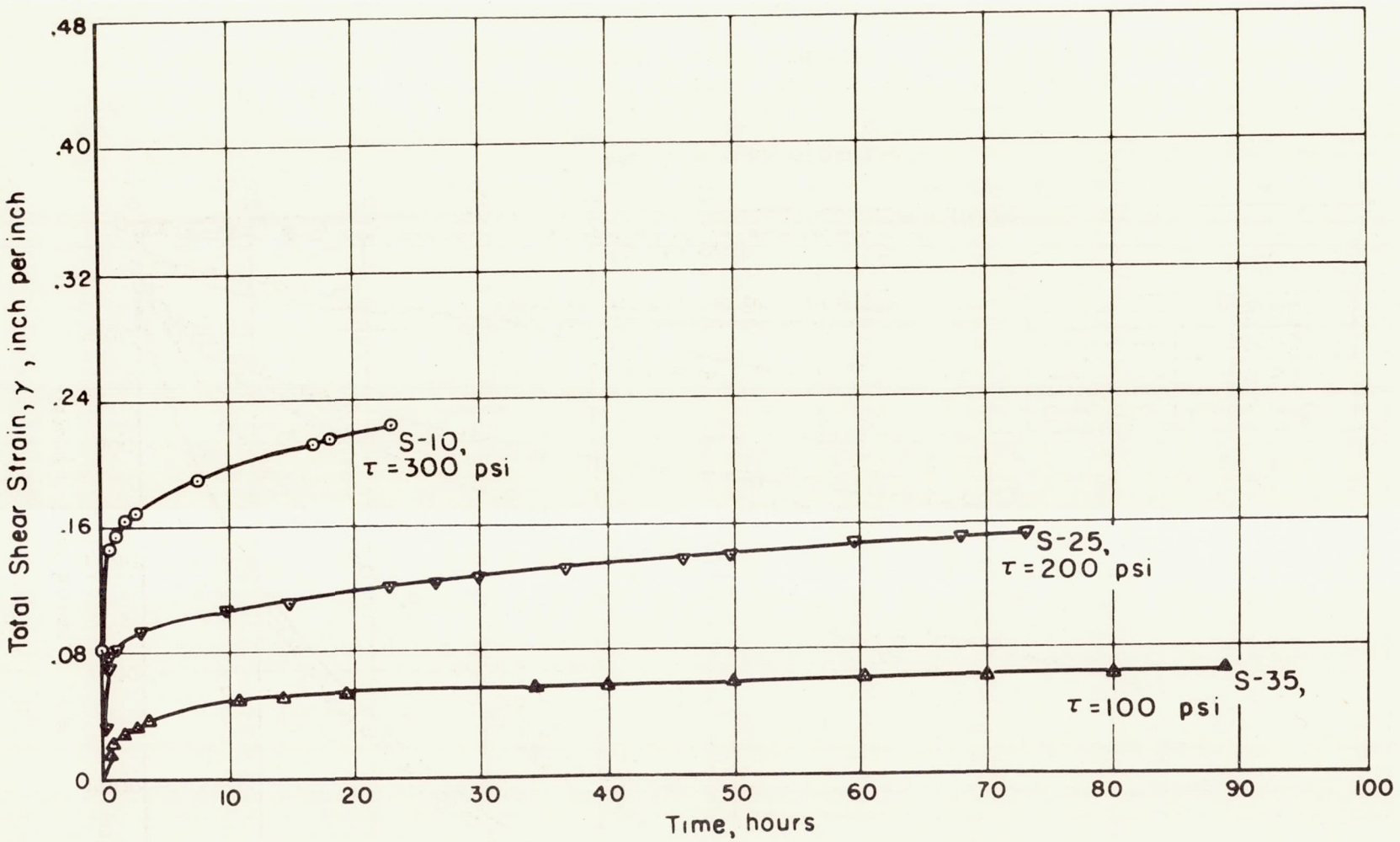


Figure 7.- Strain-time curves for three stresses at 500° F.

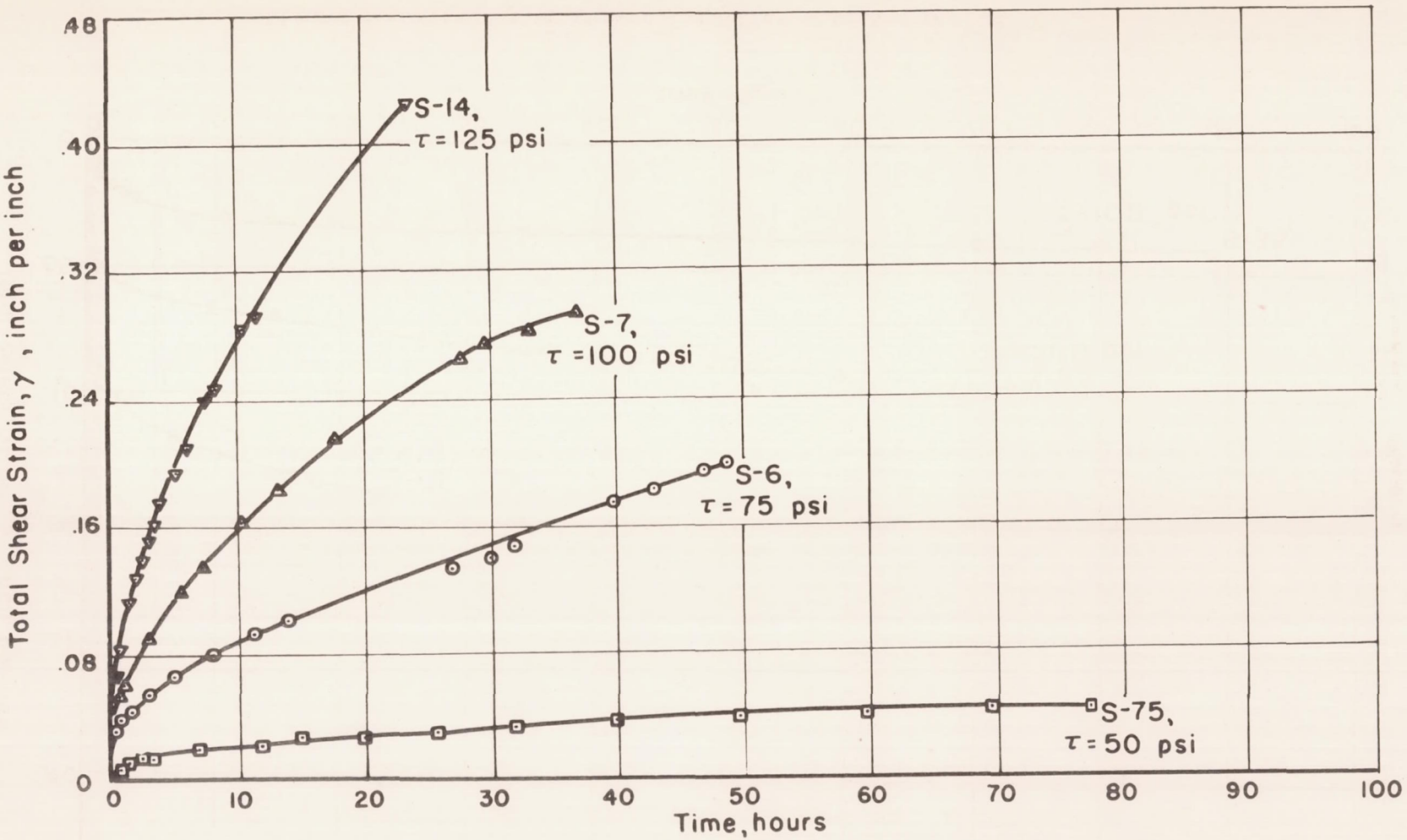


Figure 8.- Strain-time curves for four stresses at 700° F.

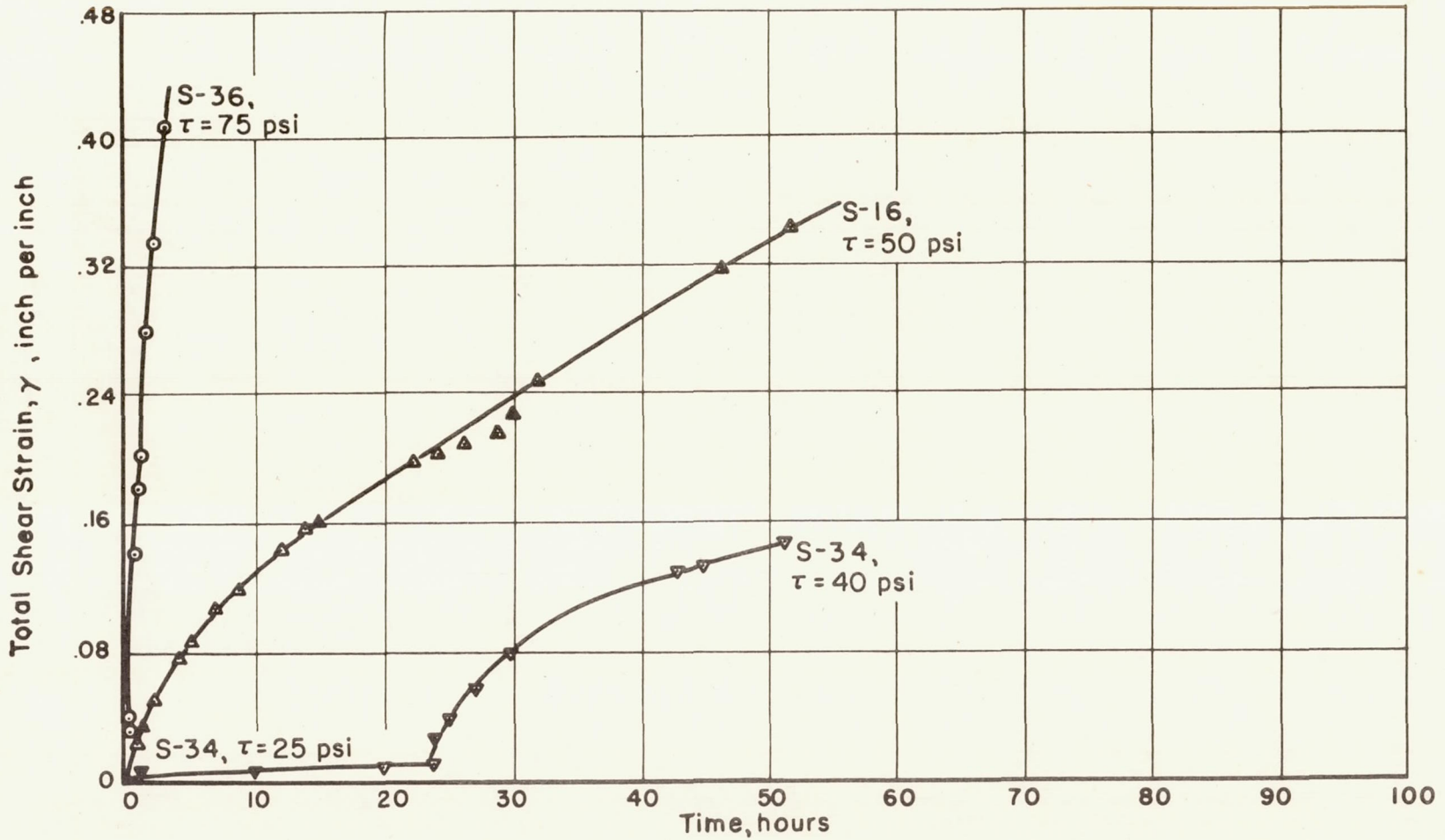


Figure 9.- Strain-time curves for four stresses at 900° F.

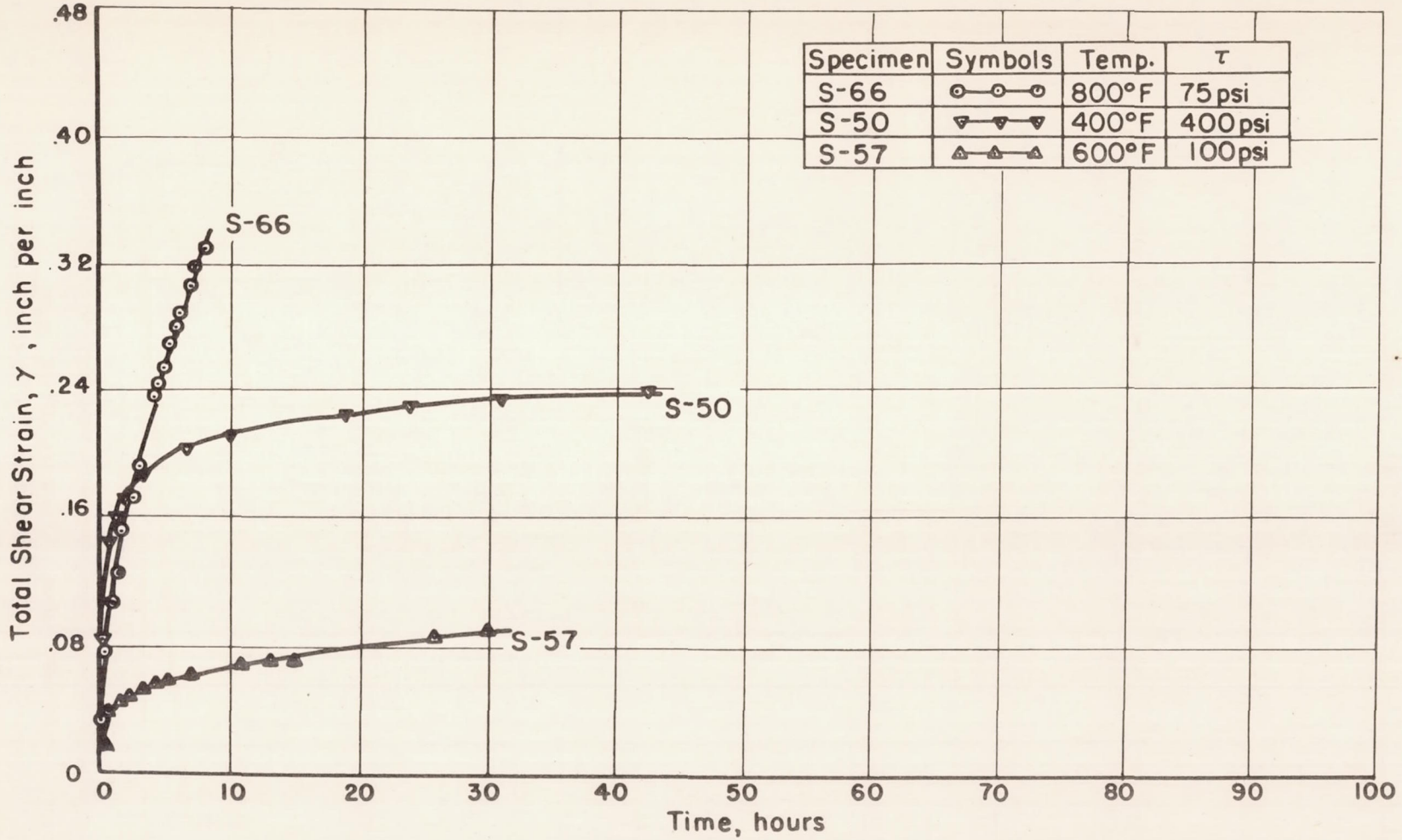
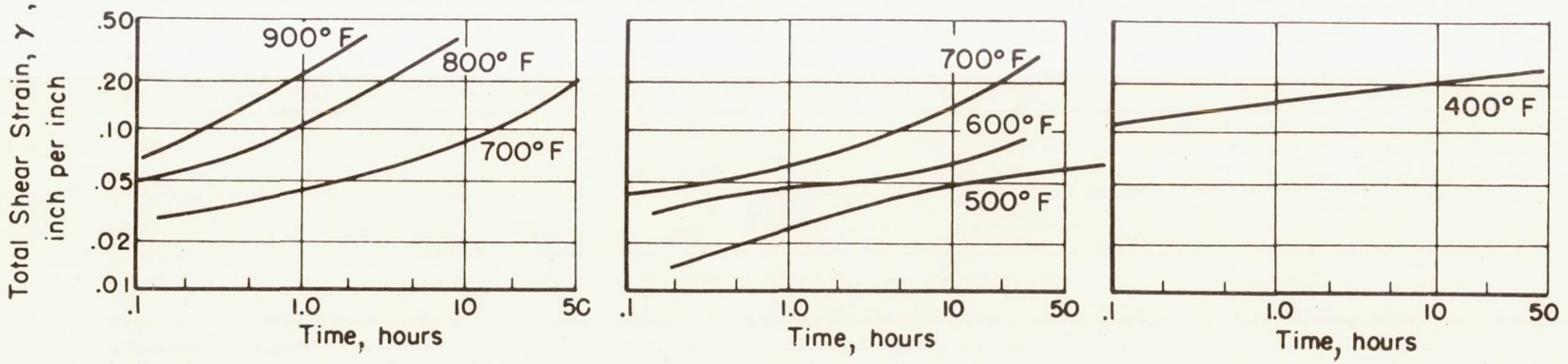


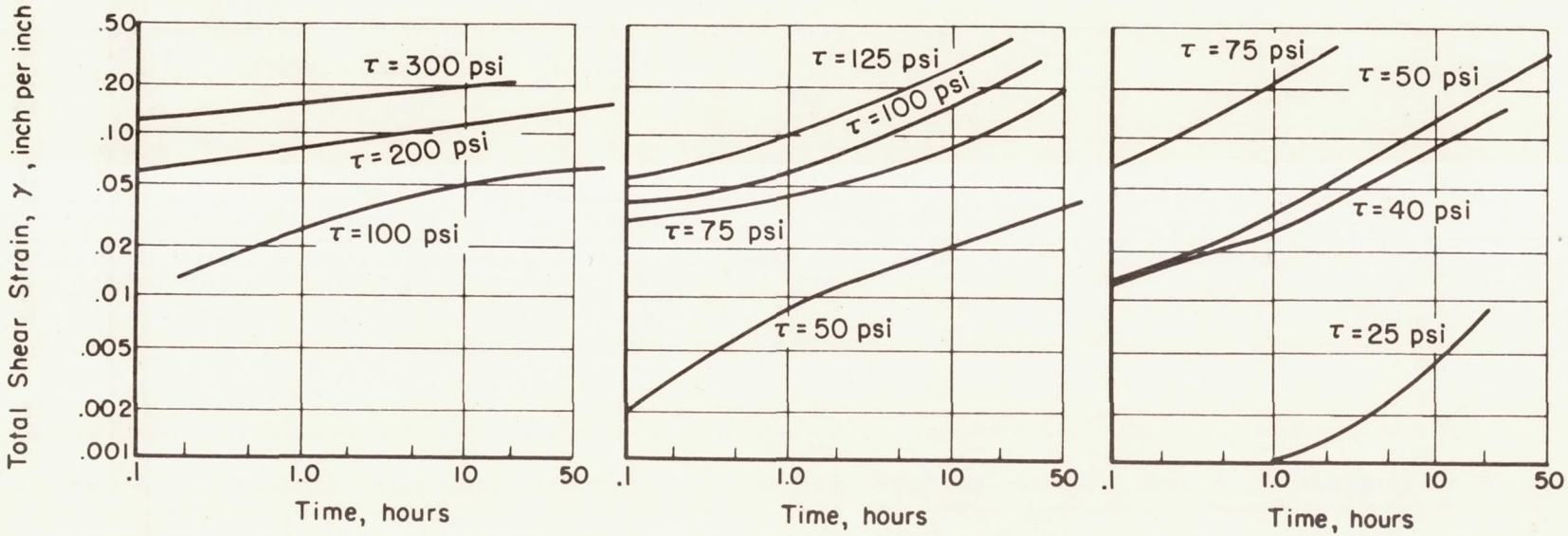
Figure 10.- Strain-time curves for various stresses and temperatures.



(a) 75-psi resolved-shear-stress tests.

(b) 100-psi resolved-shear-stress tests.

(c) 400-psi resolved-shear-stress test.



(d) 500° F tests.

(e) 700° F tests.

(f) 900° F tests.

Figure 11.- Summary of constant-stress creep data on logarithmic plots.

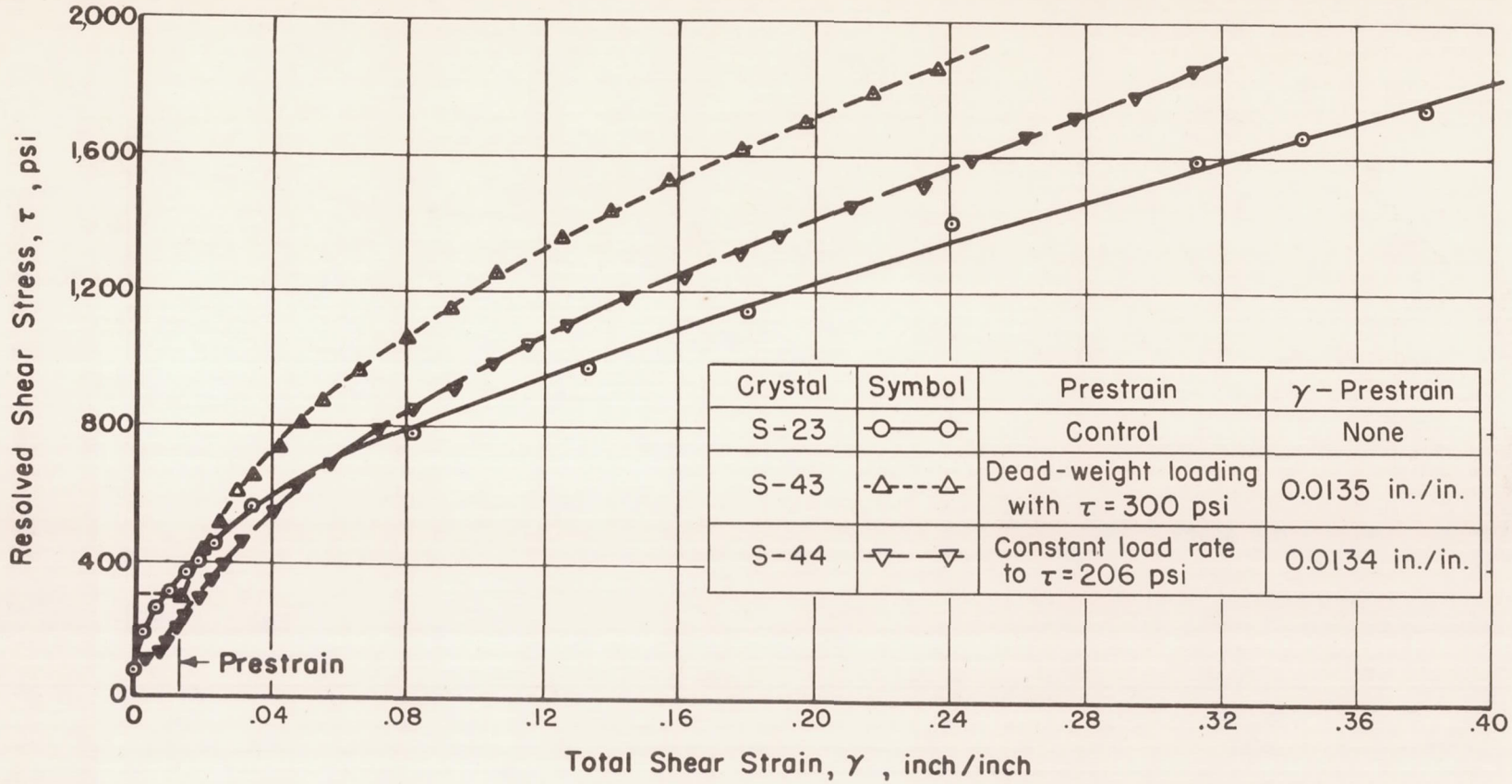


Figure 12.- Effect of prestraining by two different methods at 82° F on stress-strain curve at 82° F.

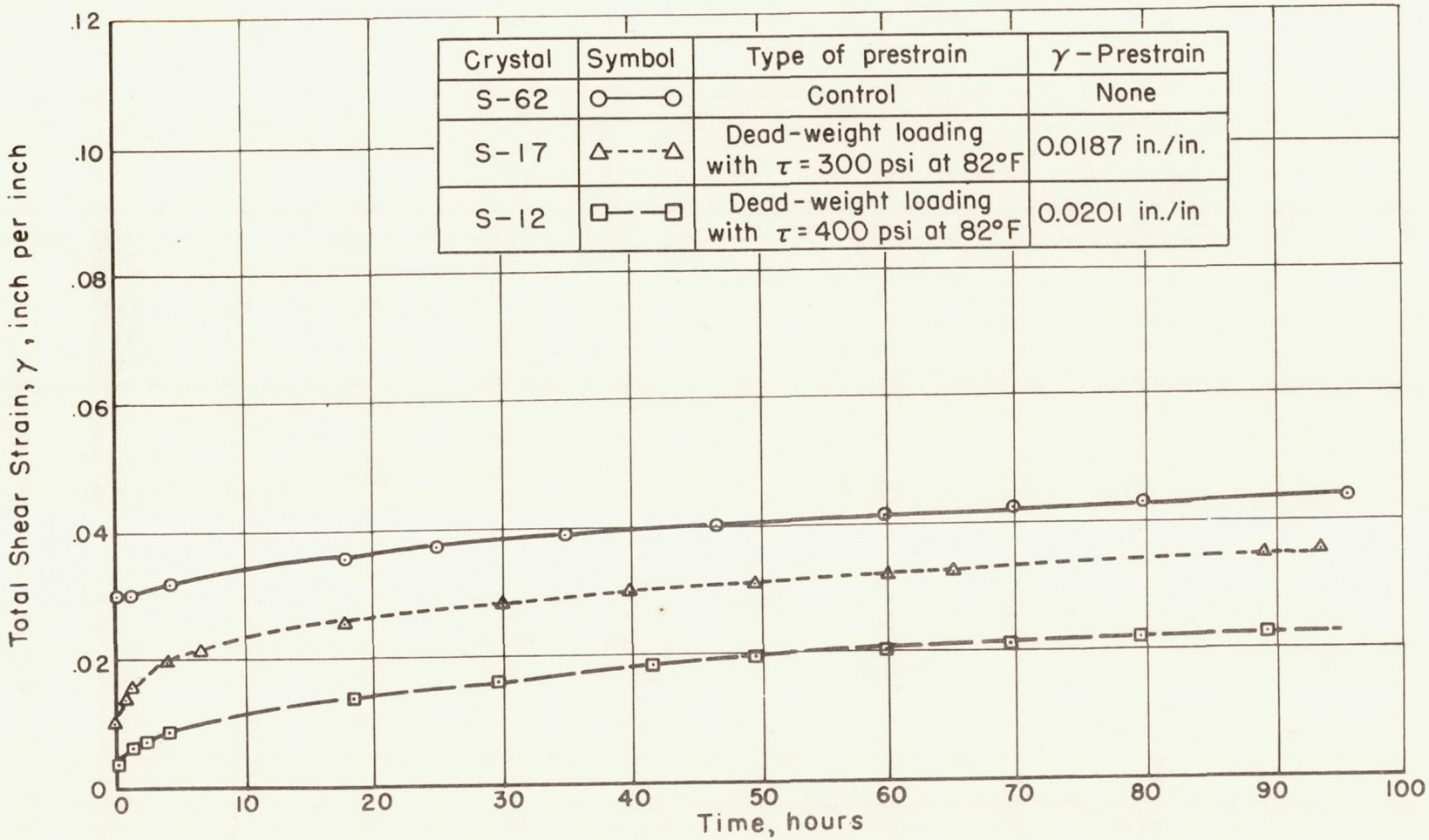


Figure 13.- Effect of rapid prestraining on creep curve at 200° F and 400-psi resolved shear stress.

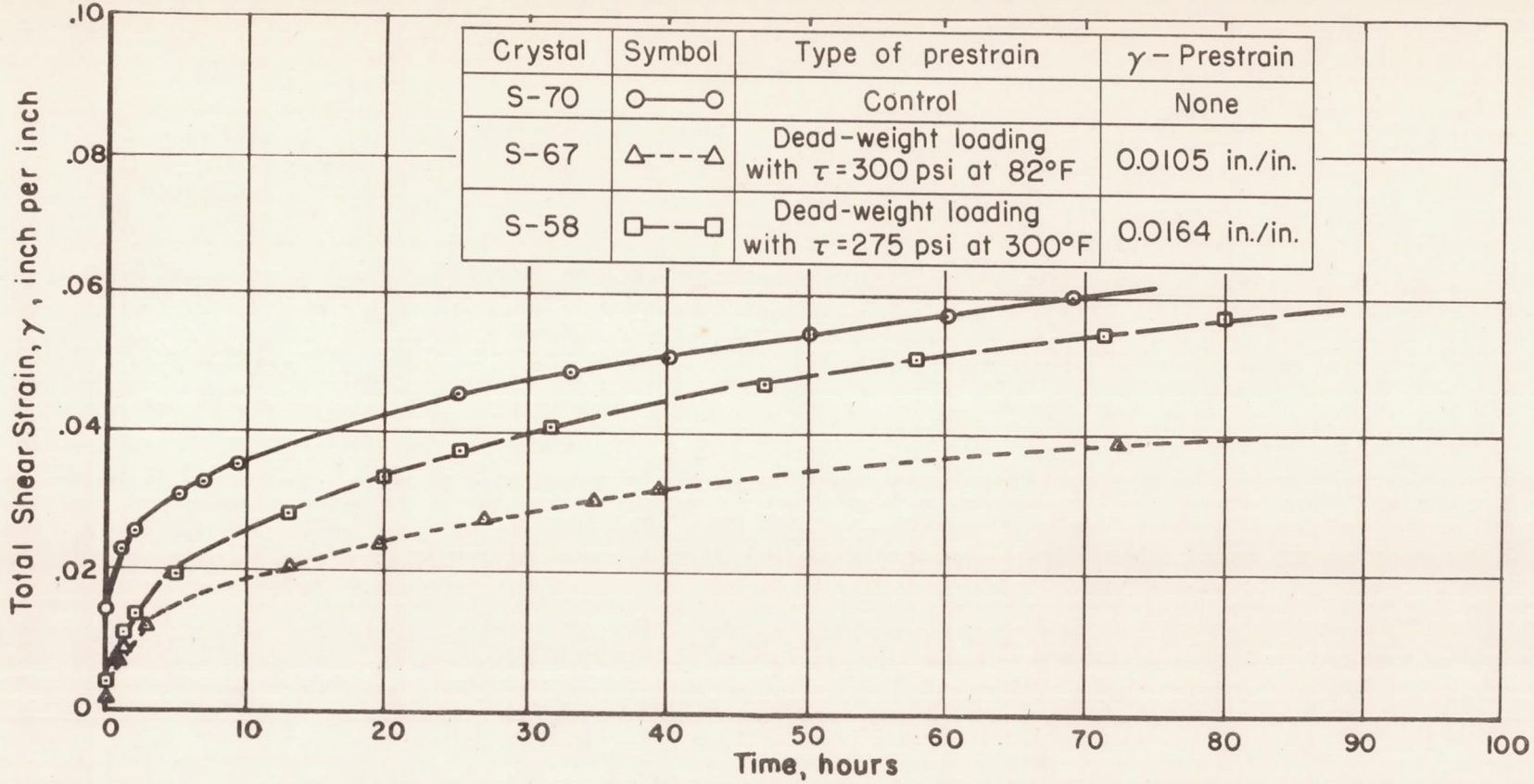


Figure 14.- Effect of temperature of rapid prestraining on curve at 300° F and 300-psi resolved shear stress.

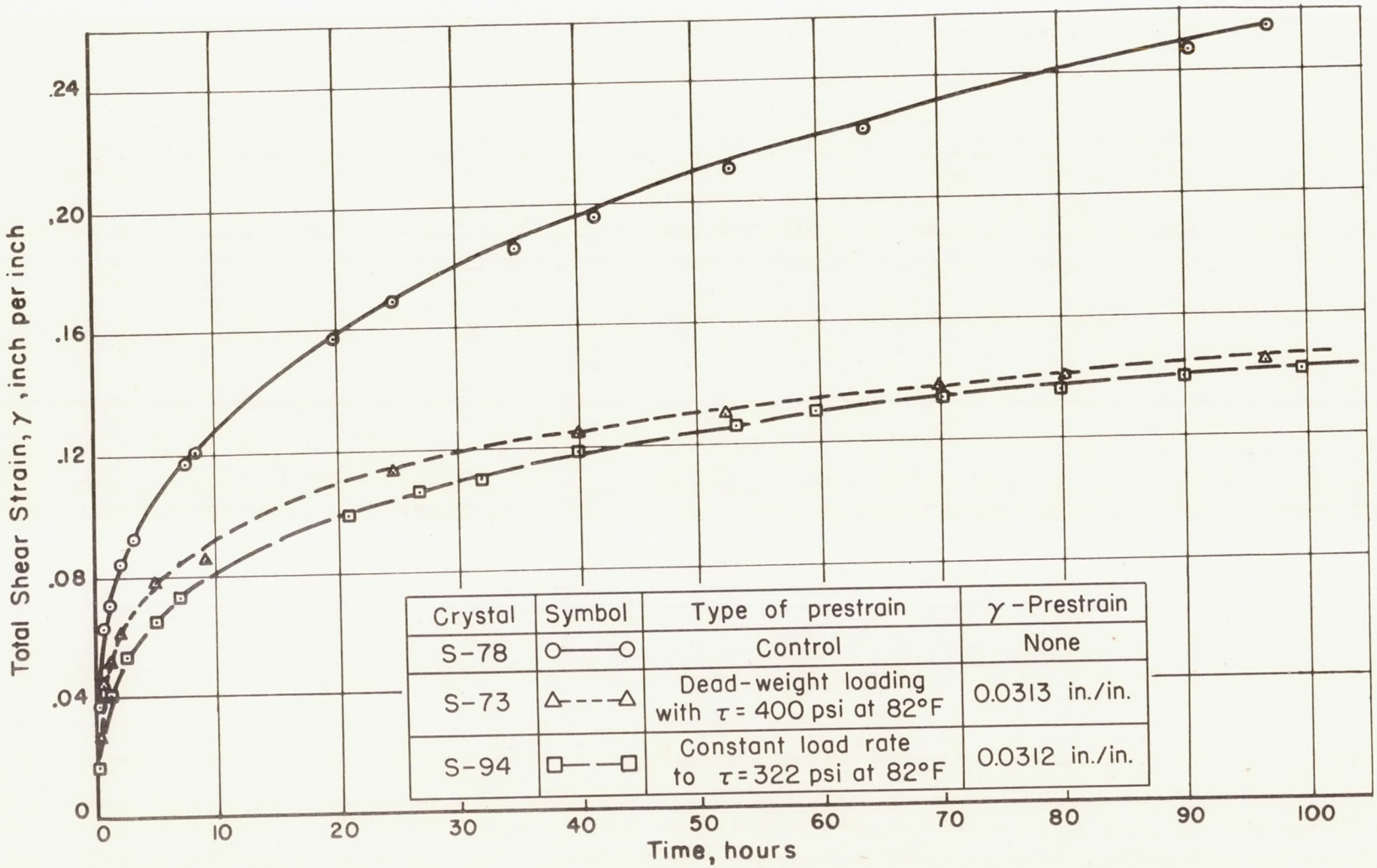


Figure 15.- Effects of two types of prestraining at 82° F on creep curve at 300° F and 400-psi resolved shear stress.

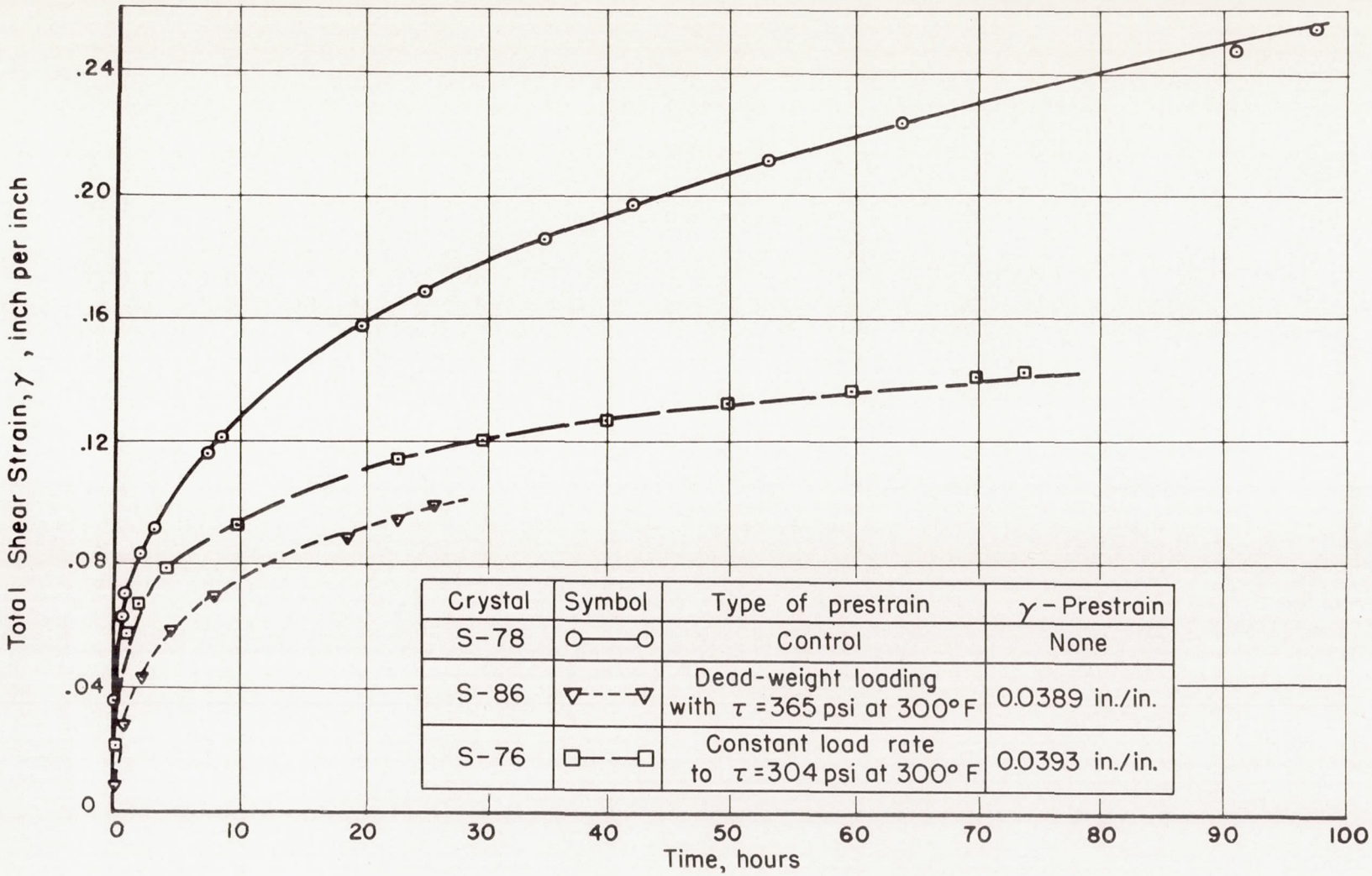
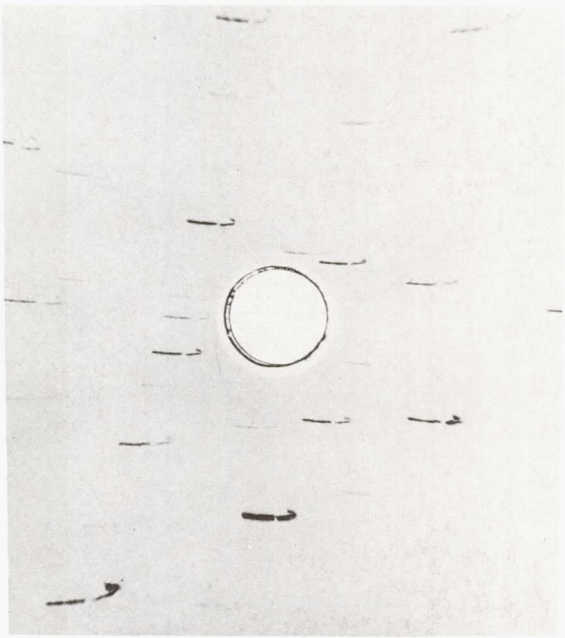


Figure 16.- Effects of two types of prestraining at 300° F on creep curve at 300° F and 400-psi resolved shear stress.



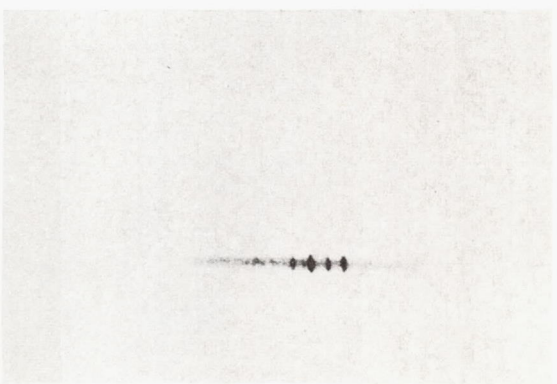
(a) Normal back-reflection Laue photograph of imperfect crystal S-63. Exposure time, 10 minutes; 1X.



(b) Back-reflection photograph of imperfect crystal S-63 with a fine pinhole and slit collimation. Exposure time, 12 hours; 1X.

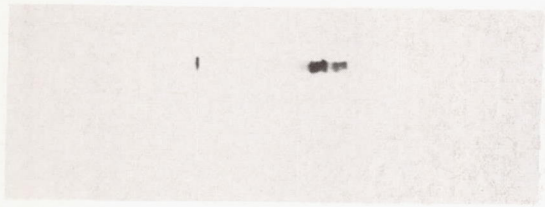


(c) Oblique Laue photograph of (200) reflection from crystal S-63. Exposure time, 20 minutes; 2.5X.

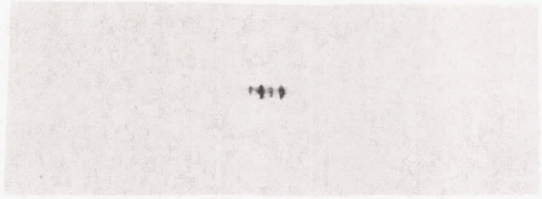


(d) Oblique Laue photograph of (200) reflection from crystal S-13. Exposure time, 10 minutes; 2.5X.

Figure 17.- Back-reflection Laue and oblique Laue photographs of imperfect crystal S-63 and oblique Laue photograph of relatively perfect crystal S-13.



(a) (200) reflection from undeformed crystal S-5 with experimental arrangement shown in figure 4. Exposure time, 10 minutes.



(d) (200) reflection from undeformed crystal S-8 with same experimental arrangement except a 150-micron pinhole was substituted for 150-micron slit. Exposure time, 100 minutes.



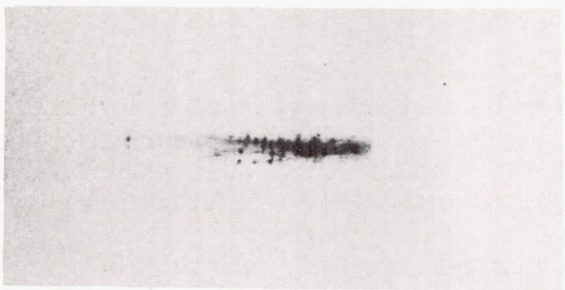
(b) Same reflection after 1.63-percent extension by prestraining with 400-psi resolved shear stress for 3 minutes at 82° F. Exposure time, 10 minutes.



(e) Same reflection after 1.53-percent extension by prestraining with 400-psi resolved shear stress for 3 minutes at 82° F. Exposure time, 100 minutes.



(c) Same reflection after an additional 11.1-percent extension by creep with 400-psi resolved shear stress at 300° F to 575° F in 17 hours. Exposure time, 80 minutes.



(f) Same reflection after an additional 7.30-percent extension by creep with 400-psi resolved shear stress at 300° F for 64 hours. Exposure time, 12 hours.

Figure 18.- Oblique Laue photographs from (200) plane of two aluminum single crystals at various stages of deformation with tungsten radiation. 2.5X.



(a) Deformation, none except a vertical and a horizontal scratch mark; exposure time, 6 hours; emulsion, type V-0; translation, 2 millimeters.



(b) Deformation, 1.47-percent extension in constant-load-rate test to 327-psi resolved shear stress at 82° F in 15 minutes; exposure time, 6 hours; emulsion, type V-0; translation, 2 millimeters.



(c) Deformation, an additional 6.94-percent extension by creep with 400-psi resolved shear stress at 300° F in 118 hours; exposure time, 15 hours (with one entrance slit removed); emulsion, lantern slide; translation, 4 millimeters.

Figure 19.- X-ray reflection micrographs from (200) plane of aluminum single crystal S-94 at various stages of deformation with copper radiation. 2.5X.

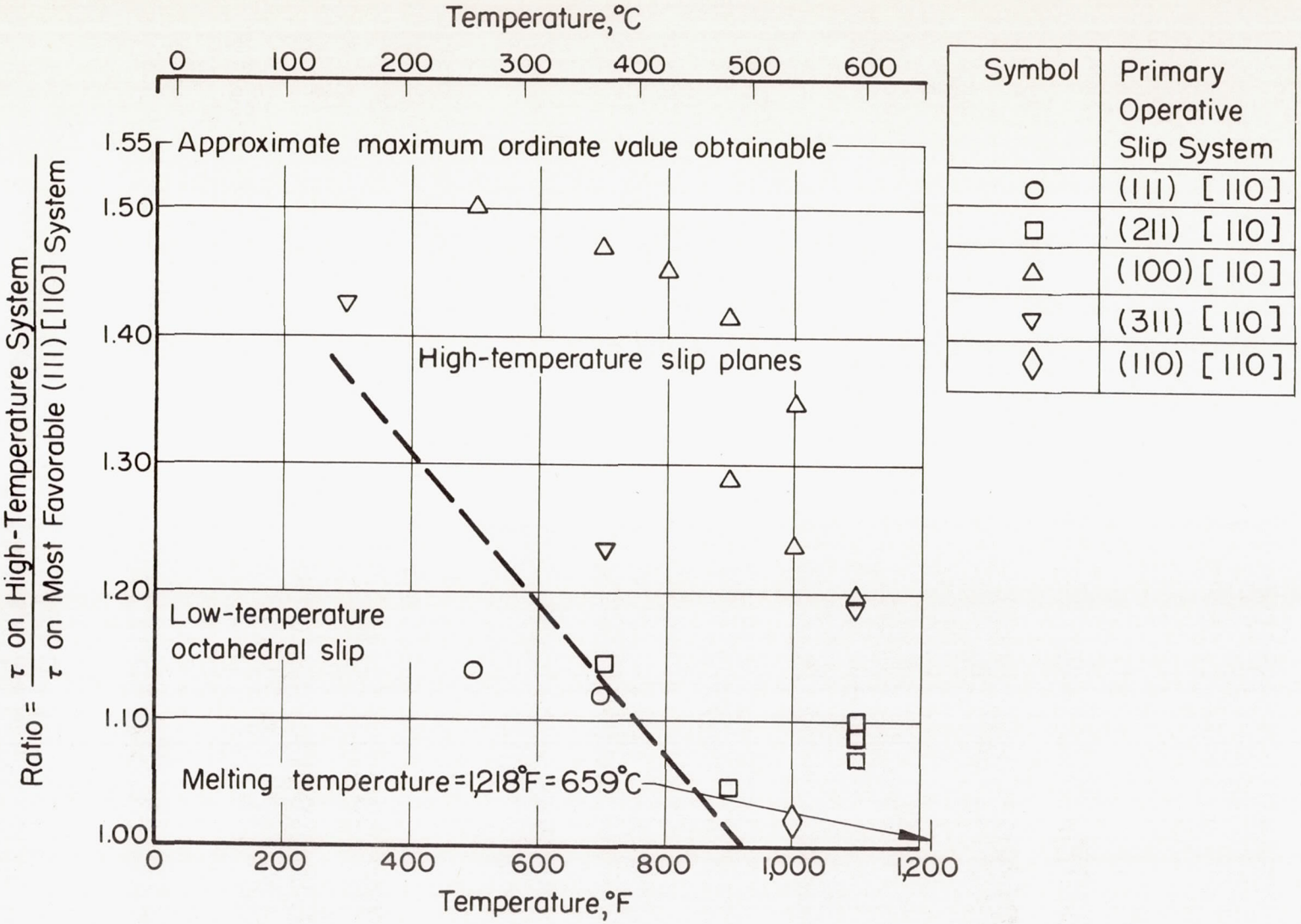
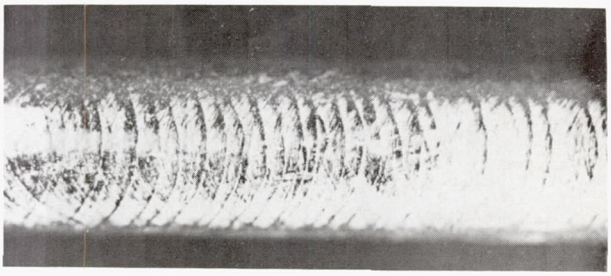
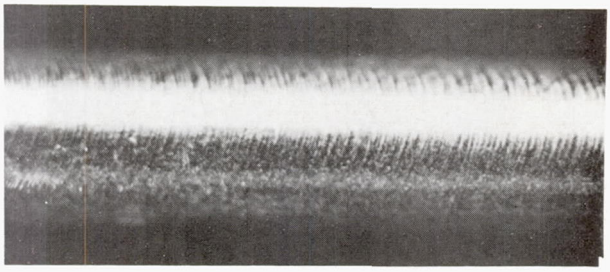


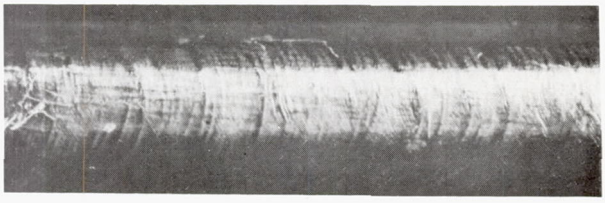
Figure 20.- Effect of orientation on operative slip system as function of temperature.



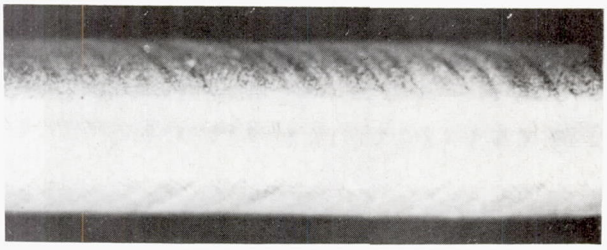
(a) Crystal S-78; test, 400-psi resolved shear stress at 300° F; extension, 12.6 percent in 94 hours.



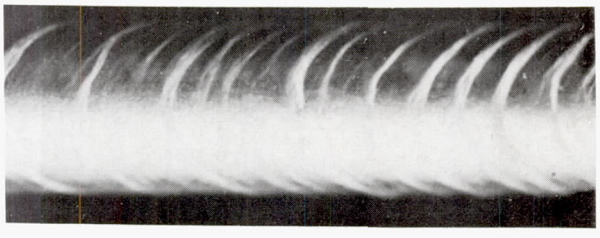
(b) Crystal S-82; test, 450-psi resolved shear stress at 500° F; extension, 7.8 percent in 140 minutes.



(c) Crystal S-18; test, 182-psi resolved shear stress at 700° F; extension, 12 percent in 46 minutes.

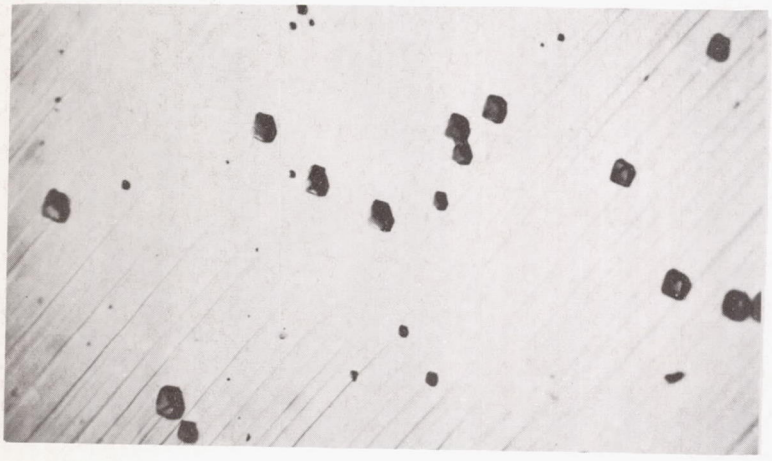


(d) Crystal S-64; test, constant load rate at 1,100° F; extension, 13 percent in 6 minutes.



(e) Crystal S-42; test, 27.6-psi resolved shear stress at 1,100° F; extension, 14 percent in 5.2 hours.

Figure 21.- Light micrographs of kink bands and slip bands on single crystals of aluminum deformed at various temperatures. 2X.



(a) Crystal S-78; test, 400-psi resolved shear stress at 300° F, extension, 12.6 percent in 94 hours; typical kink band.



(b) Crystal S-82; test, 450-psi resolved shear stress at 500° F; extension, 7.8 percent in 140 minutes; sharp kink bands.

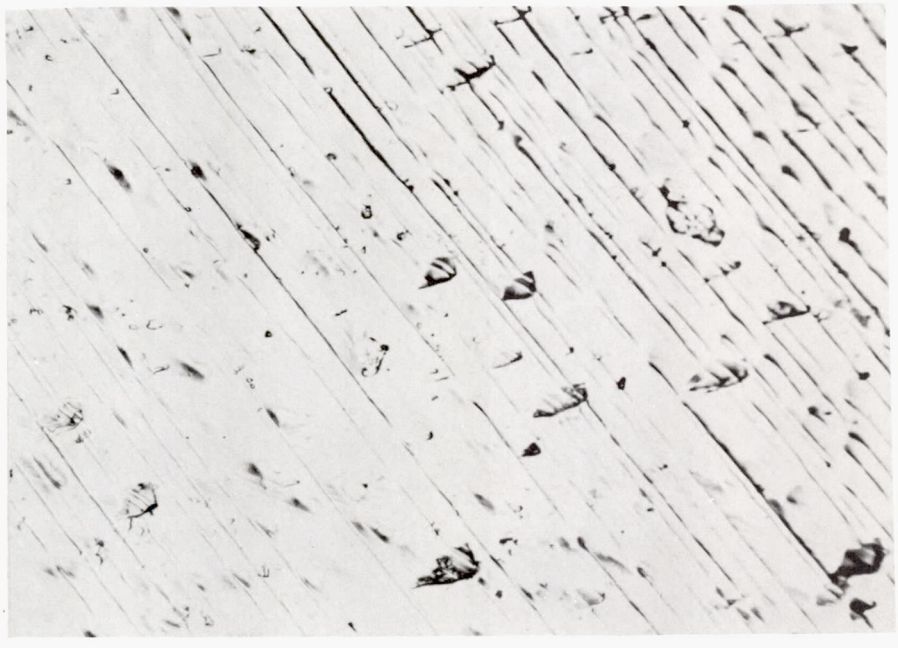


(c) Crystal S-51; test, 600-psi resolved shear stress at 500° F; extension, 15 percent in 1 minute; duplex slip in kink bands.

Figure 22.- Light micrographs of various types of kink bands observed on unshadowed Faxfilm replicas of deformed aluminum single crystals. 100X.



(a) Crystal S-2; 100X. (See fig. 26 for electron micrographs.)



(b) Crystal L-12; 250X. (See fig. 27 for electron micrographs.)

Figure 23.- Light micrographs of slip bands on deformed aluminum single crystals of two purities with chemically polished surfaces. Both micrographs are from unshadowed Faxfilm replicas.



(a) Crystal P-181; test, 400-psi resolved shear stress at 82° F (10 minutes); extension, 0.90 percent; 13,500X.



(b) Crystal P-175; test, tensile test at 400° F in vacuum; extension, 5 percent; 8,000X.



(c) Test, bending at 82° F; deformation, heavily deformed; 3,500X.

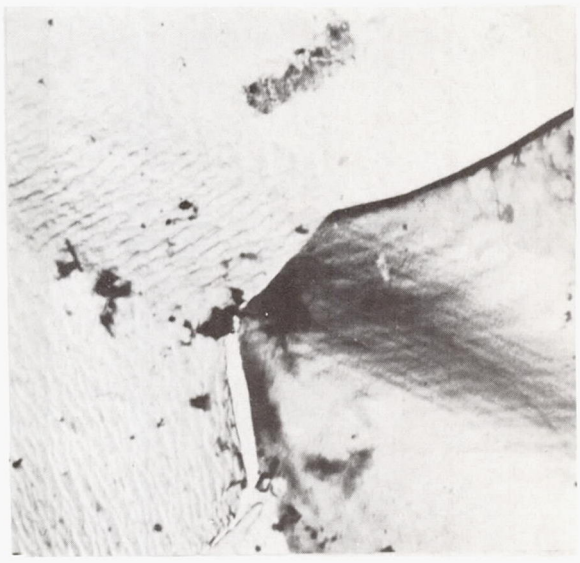


(d) Test, bending at 82° F; deformation, heavily deformed; 4,500X.

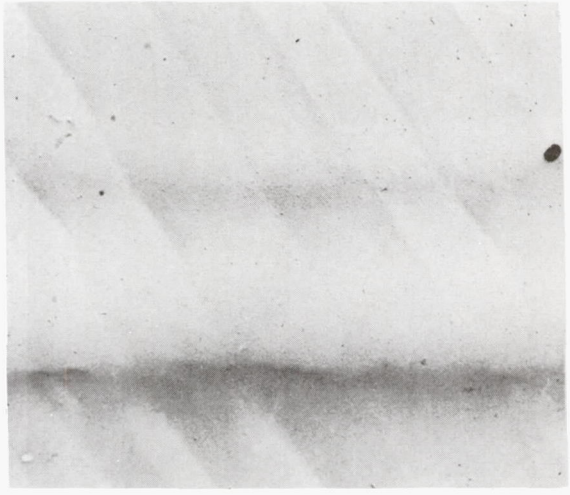
Figure 24.- Electron micrographs of aluminum-oxide replicas from electropolished surfaces of deformed aluminum single crystals.



(a) Crystal S-89 (unoriented); test, 800-psi tensile stress at 500° F in vacuum; extension, 11 percent in 19 hours; type replica, aluminum oxide; 7,500X.



(b) Crystal S-56; test, constant load rate at 500° F with oil coating; extension, 22 percent in 16 minutes; type replica, aluminum oxide; 4,000X.



(c) Crystal L-11; test, 970-psi resolved shear stress at 500° F in vacuum; extension, 12.4 percent in 17 hours; type replica, Formvar; 3,000X.

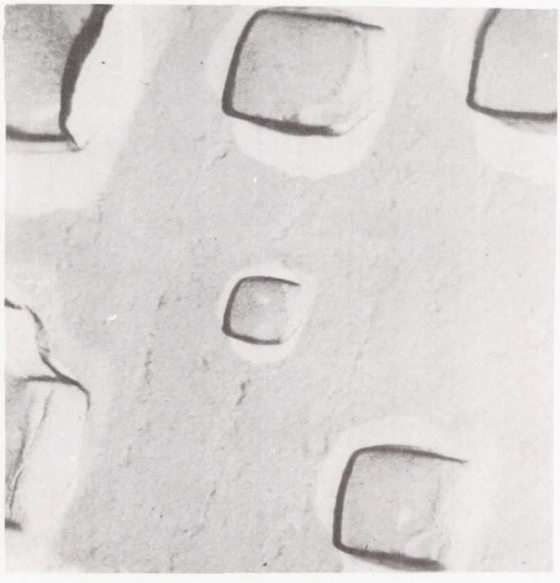


(d) Crystal L-11; test, 970-psi resolved shear stress at 500° F in vacuum; extension, 12.4 percent in 17 hours; type replica, platinum; 4,000X.

Figure 25.- Electron micrographs of slip bands on various replicas from electropolished surfaces of deformed aluminum single crystals.



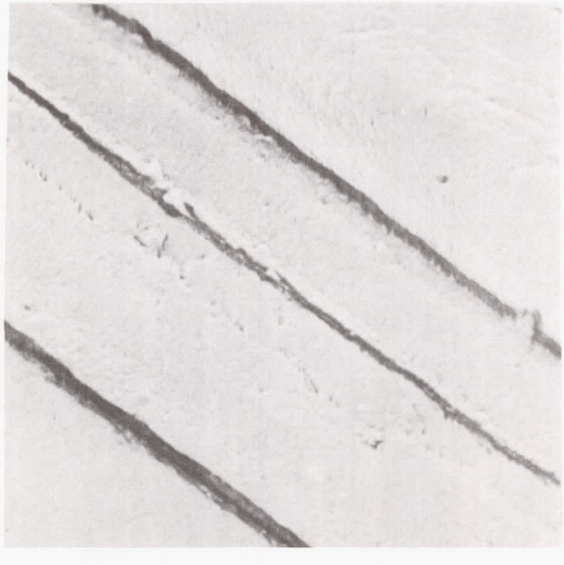
(a) Crystal S-2; undeformed; surface, chemically polished and etched; 6,500X.



(b) Crystal S-2; undeformed; surface, chemically polished and etched; 16,000X.



(c) Crystal S-2; test, 400-psi resolved shear stress at 500° F with oil coating; extension, 9.3 percent in 1.5 hours; surface, chemically polished; 23,000X.



(d) Crystal S-37; test, 50-psi resolved shear stress at 1,000° F in vacuum; extension, 12 percent in 1.4 hours; surface, electropolished; 21,000X.

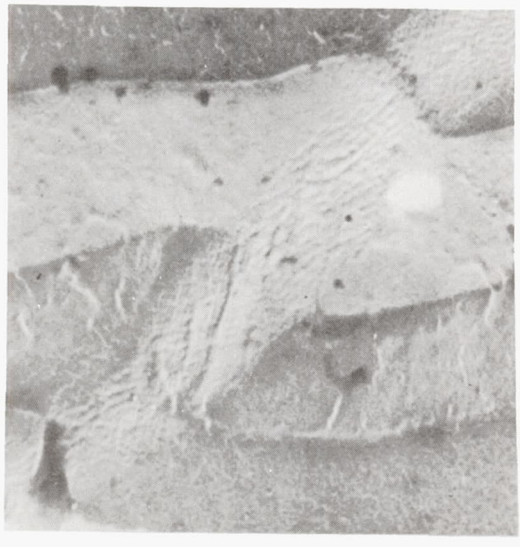
Figure 26.- Electron micrographs of platinum replicas of undeformed and deformed regions on aluminum single crystals.



(a) 14,000X.



(b) 14,000X.



(c) 14,000X.



(d) 50,000X.

Figure 27.- Electron micrographs of slip bands on a deformed aluminum single crystal with a chemically polished surface. Crystal L-12; test, constant load rate at 500° F with protective oil coating; extension, 14.4 percent in 19 minutes; type replica, platinum.